Polymer-Mediated Interactions and Phase Behaviour of Polymer-Particle Dispersions

Haddadi, Sara

2022

Document Version:
Publisher's PDF, also known as Version of record

Polymer-Mediated Interactions and Phase Behaviour of Polymer-Particle Dispersions

SARA HADDADI | DIVISION OF THEORETICAL CHEMISTRY | LUND UNIVERSITY

Polymer-Mediated Interactions and Phase Behaviour of Polymer-Particle Dispersions

Polymer-Mediated Interactions and Phase Behaviour of Polymer-Particle Dispersions

Sara Haddadi

LUND
UNIVERSITY

Thesis for the degree of Doctor of Philosophy
Faculty opponent: Johan Bergenholtz

To be presented, with the permission of Lund University, lecture hall A at the center for Chemistry and Chemical Engineering (Kemicentrum) on Friday, the 10th of June 2022 at 9:15.

Organization
LUND UNIVERSITY
Department of Chemistry
Box 124
SE-221 00 LUND
Sweden

Document name
Doctoral Thesis

Date of disputation
2022-06-10

Sponsoring organization

Author(s)
Sara Haddadi

Title and subtitle
Polymer-Mediated Interactions and Phase Behaviour of Polymer-Particle Dispersions:

Abstract
Interactions between colloidal particles can be modelled by particles grafted with polymers. In this work, structural and physical properties of colloids are investigated under variation of parameters such as pH, ionic strength, and temperature, where aggregation and cluster formation can be monitored in aqueous solution. Being the subject of our work, in particular, we show that linear or polymer-like clusters can be formed if long-ranged repulsive barriers are combined with very short-ranged attractive minimums stimulating particles to form highly anisotropic structures. This is adjusted by changing the properties of particles and the dispersing medium. Besides, we utilize Metropolis Monte Carlo (MC) simulation to investigate the behavioural change of these particles with a focus on the types of clusters formed. A simplistic potential of mean force is adopted for the simulations, but we also invoke a more elaborate model, to demonstrate that similar interactions can be obtained when the grafted chains are treated explicitly. An important criterion in these studies is that the particle size is large enough to allow structural analyses via microscopy. The range of electrostatic interactions is adjusted by the ionic strength, and the strength of the short-ranged attraction is changed via hydrophobicity regulation of the grafted layer through temperature variation. The results revealed that highly anisotropic structures which resemble linear or branched polymers were the clusters at equilibrium. We could also investigate the effect of polymer addition to the particle dispersions. We could detect a non-monotonic temperature dependent aggregation of particles from attraction to repulsion to attraction, where the polymer-mediated interactions were repulsive. The results were validated against experiments.
The next phase of this work is devoted to the study on capillary induce phase transitions with an experimental focus on polymer solutions containing PNIPAM at the presence of hydrophobic surfaces (mesoporous silica) as a function of pH, temperature and chain length. The capillaries/confined geometries are known to influence the phase diagram of polymer solutions where condensation of bulk solutions may occur close to the surfaces. This work is performed using a combination of experiments and theories where a shift to the LCST (lower critical separation temperature) is presumed to occur, resulting in a capillary-induced decrease in the LCST.

Key words
Particles, Stability, Phase transition, Simulations, Experiments, Capillary induced phase transition, Polymer solution, Phase diagram, Surface effects

Classification system and/or index terms (if any)

Supplementary bibliographical information

Language
English

ISSN and key title

ISBN
978-91-7422-893-9 (print)

Recipient's notes

Number of pages
139

Price

Security classification

Polymer-Mediated Interactions and Phase Behaviour of Polymer-Particle Dispersions

Sara Haddadi

LUND
UNIVERSITY

Cover illustration front: Image by Sara Haddadi

Funding information: This work was financially supported by Swedish Research Council

Faculty of Science, Department of Chemistry

ISBN: 978-91-7422-893-9 (print)

Printed in Sweden by Media-Tryck, Lund University, Lund 2022

Media-Tryck is an Nordic Swan Ecolabel certified provider of printed material. Read more about our environmental work at www.mediatryck.lu.se

MADE IN SWEDEN

Dedicated to my parents

Contents

List of publications

1 **Building polymer-like clusters from colloidal particles with isotropic interactions, in aqueous solution**
S. Haddadi, M. Skepö, P. Jannasch, S. Manner, J. Forsman
Journal of Colloid and Interface Science, 2021, 581, pp. 669–681

2 **Polymer-Like Self-Assembled Structures from Particles with Isotropic Interactions: Dependence upon the Range of the Attraction**
S. Haddadi, H. Lu, M. Bäcklund, C. E. Woodward, J. Forsman
Langmuir, 2021, 37, pp. 6052–6061

3 **From Attraction to Repulsion to Attraction: Non-monotonic Temperature Dependence of Polymer-Mediated Interactions in Colloidal Dispersions**
S. Haddadi, M. Skepö, J. Forsman
ACS Nanoscience AU, 2021, 1, pp. 69–80

4 **Confinement-induced fluid-fluid phase transitions in simple fluid mixtures, under bulk supra-critical conditions**
S. Haddadi, C. E. Woodward, J. Forsman
Fluid Phase Equilibria, 2021, 540, pp. 112983

Acknowledgements

Writing this part of the thesis is thinking of four years life. I cannot begin to describe my feelings toward this journey. Working and living in a new environment, can be an overwhelming experience, yet I have been surrounded by great people who made it incredibly joyful, and peaceful for me to fit in and find my place, and I will do my best to thank them. First and foremost, I would like to express my gratitude to my supervisor, Jan, for all of his support, kindness, guidance, and patience. What better way to show your support other than looking at your first email to me when I was about to land in Sweden for the very first time, a thorough description of how to get to Lund, then picking me up at the train station and making sure that I am settled in, from that moment, I always felt I can count on your full support in every way and I am so grateful about it. Theoretical chemistry could be challenging especially for me, coming from a different background with more focus on experimental studies, but your brilliance, knowledge and expertise in what you do, especially in programming, helped me immensely during this time. Thanks to your expertise, there was nothing complicated when we had scientific discussions. I always felt that I can count on you in whatever comes along the way, and you were my mentor, role model, and great friend. I simply cannot thank you enough.

I want to thank my supervisors on the experimental part of my thesis. Great thanks dear Marie, you never hesitated to support me in any imaginable way, you were always there to guide me in my research. You are a brilliant scientist, a great mentor, and most importantly a great friend. Special thanks to Sophie, you helped me to set up my experiments, thanks for many discussions we had during these years.

Great thanks Michael for your supports your assistance, when facing a problem, with your expertise which made it easier for us to set up things and to fix the errors. Great thanks to Patric for the useful suggestions regarding my experiments, you are an expert and I knew if I contact you, I could find best possible solutions to the problems. Great thanks to Maria for the purchases as well as nice chats we had for different occasions which is greatly appreciated. So much thanks Helena and Maria for the administration helps!. It was my chance to meet great people with diverse background showing me that life is not just work

and scientific progress but living and setting up higher standards for yourself. All of you at the department helped me widening my world view in different ways and helped me to grow as a person. I wish all of you all the best in your professional and personal lives.
Finally I like to thank my parents for their love and supports which brought me here. My lovely sister, Leila, you are the greatest soul I have ever known thanks for being such.

Popular summary

Polymers are chain-like molecules composed of connected monomers with different conformations. Depending on their properties, polymers between surfaces can generate repulsive or attractive forces. If we consider a particle dispersion, this means that the presence of polymers can either ensure that the particles stay apart, or force them together into aggregates. The 'polymer-mediated interactions', their characteristics and behaviours still need to be properly modelled. By applying different polymers in different conditions in experimental approaches, we can explore and model different mechanisms associated with particle aggregation.
Colloids are particle dispersions, where the particles have a size ranging from 10 nm to about 1 μm. These dispersions can be used as models to study "phases", such as gas-like to solid-like dispersions. These models then can be used to describe interactions in atomistic and molecular scales where rapid motions and small length scales cannot be captured in experiments. Different polymers and varying conditions such as temperature, acidity, salt concentration, etc. can be used as regulating parameters. Transitions between different "phases" are related to the physical conditions and properties of solutes such as polymers mediating the particle interactions which in turn results in changes to the macroscopic properties of the dispersions.
Using a combination of both theory and experiments, we focus, in the first part of this thesis, on understanding interparticle interactions in colloidal dispersions, in the presence of polymers. Polymer-mediated interactions, generated by thermoresponsive polymers, can cause both stabilization and destabilization of the dispersions, depending on the temperature. This has been thoroughly investigated in the thesis, including effects from grafted and dissolved polymers in the particle dispersions.

In addition to these polymer-mediated interactions, the polymer solution itself can separate into polymer-rich and polymer-poor phases. These phases may be influenced by confinements which is relevant in porous media. This is the focus of another part of this work.

Chapter 1

Introduction

In this chapter, we summarize general terms and issues related to polymer/particle dispersions with special consideration of colloids. The aim is to provide the necessary framework for starting and establishing our analyses. Experiments and simulations will then be combined to investigate the behavioural properties of these dispersions. Beside this, the summary of the results will be discussed separately in a concluding section. We find colloids in many applications from food and cosmetics to suspensions, biological fluids, etc. In all these applications, particles or droplets are dispersed in a solvent. The quality and stability of colloidal dispersions relies not only on the properties of each phase, but also on physiochemical conditions, such as temperature, and pH. In order to prepare a dispersion with desirable properties, intermolecular interactions at microscopic scales should be assessed. This can be achieved by a combination of experiments and simulations.
Interactions between colloidal particles (solid particles) or flat surfaces, can be regulated by addition of polymer, or by changing the pH and ionic strength of the dispersant. External stimuli, such as temperature or electric field, can also be used for tuning the interparticle interactions. In this work, we aim to study the behavioural changes of dispersions containing particles and polymers, where phenomena such as adsorption and phase transitions can be investigated. The main mechanism involved here is polymer-mediated interactions such as depletion/bridging interactions whose strength and range are regulated by parameters such as polymer length, pH and temperature.[1]

Colloidal particles and soft matter

Colloids are dispersions containing particles with size ranging from 10 nm to 1 μm. Due to their relatively large size, they have been used as model systems to study interactions and structural properties in soft matter, where the time and length scale of motions (as compared

with atomic scale) allow us to apply techniques such as microscopy for investigation.[2] Colloidal particles undergo Brownian motions as a result of their thermal movements and collisions with solvent molecules. Under the influence of forces, such as gravitational or interparticle attractions, particles may start to form aggregates or phase separate irreversibly when coming into contact. Methods to prevent aggregation include modification of dispersion properties, for instance by introducing charges or polymer grafting of surfaces. The latter approach will be explained in the next chapters. Even though kinetic effects often are relevant, we mainly investigate thermodynamics of aggregation in this work, by addressing free energies of dispersions which can be defined from repulsive and attractive forces between the particles counteracting to produce a variety of responses. Such interactions, and the resulting effects on arrangements of particles, will be discussed in the next chapter. Here, however, we merely mention that due to the many parameters affecting colloidal stability, their phase diagram is often rich in terms of types of phases and structural properties such as particle packing. Hard spheres are well known simplified models in this context, which are interacting with no forces except when they are at contact. Examples of these can be sterically stabilized particles. Hard spheres have been used as a basis of soft matter studies, where gas to crystalline phases are formed only as a response to a change of the volume fraction. [3, 4] In a more complex system, things are more complicated and many parameters may influence the interactions and thereby the resulting structures of particles, with solvent quality, pH, salinity, temperature, etc being a few examples. The complexity is even more evident when dealing with soft particles (gel) with networks and size changing upon varying any other parameters. In comparison with the hard spheres having fixed size, scrutinizing the mechanisms upon decomposing the effects can be a difficult task in understanding and modelling of these transitions. [5–7]

The synthesis of particles is another important task for constructing colloids with desirable responses, for a given application. The synthesis involves preparing particles varying in morphology, size and shape, and surface chemistry. Various methods can be used for synthesizing particles. In the context of directed assembly, we can mention janus and patchy particles whose inherent asymmetry and anisotropy in shape generates anisotropy in the resulting structures. [2, 8, 9] In addition to these, identical, radially symmetric, particles are also relevant. These particles are often prepared for homogeneous distributions in dispersions, for instance core-shell particles in a dispersing matrix, for constructing a well structured composite having suitable properties.[10–15] Despite their spherical shapes, they can associate into anisotropic clusters showing different degrees of directionality, which occur due to the changes in the interparticle interactions as a response to internal or external parameters controlling the shape of clusters. In case of composite materials, the inhomogeneity in particle distribution often causes defects in the structure and the strength of the composites. In emulsions and dispersions too the stability is dependent on the particle distribution. This underlines the importance of structural pattern within the dispersing

matrix. In many cases of grafted particles, in aqueous or non-aqueous solvent, directionality has been observed, introducing various phases.[16–18] For instance, in cases where grafted particles are immersed in polymer matrices, the anisotropy often stems from short-ranged attractive interactions, from H-bonding, depletion or hydrophobic interactions, and entropic forces generated from the constituent chains, inducing a long-range repulsive potential. [19] Despite the studies on anisotropy in polymeric matrices, structural properties of particles dispersed in non-polymer matrices has not been fully investigated and studies on these systems are quite sparse, especially in experiments.[20–22] This is the subject of our first work in this thesis, where parameters influencing formation of such clusters will be investigated.
Using a combination of experiment and theory, we aim to investigate properties of polymer/particle dispersions. Even though this can span from liquid-like to solid-like dispersions and further gel structures, we focus on the dilute regime with the aim to study anisotropy. In a separate work, we also investigate phase transitions of solutions in confined spaces. Effects of polymers on interactions and phase transitions will be studied. Therefore, the work will be summarized into two main projects. Short explanations of terms used in each study is highlighted below. The synthesis, experiments and theory are introduced in later chapters.

1.1 PEG-grafted polystyrene particles

The stability of colloids can be regulated by balancing out the intermolecular interactions in the dispersion. Any change causing destabilization of the dispersion can be associated to a change in internal or external parameters (such as temperature or solutes added to the dispersion, etc. influencing the interparticle interactions). Particles often carry charges or grafts yielding repulsive forces which in turn increase the stabilities.[6, 7] The choice of techniques and conditions while synthesizing particles can be all regulated, in order to prepare a dispersion with suitable properties. In this context, a vast variety of particles, organic or inorganic, have been synthesized using different techniques for various applications. In the case of polymeric particles, emulsion and dispersion polymerization or grafting-to have been widely used, both to synthesize, and to modify the surface chemistry as a post-synthesis modification.[23, 24] This will be discussed further in the next chapters.
Polymerization of particles occurs through a nucleation/growth process so that a nuclei can form from a chemical exchange of monomer with bulk counteracting the surface energy term which results in particle growing in size to the point where constant values for size is achieved at equilibrium. The size can be then regulated by the physiochemical conditions. In a similar way, the assembly and stability of particles, can also be controlled using physiochemical conditions which cause changes in the interactions between the particles.
Due to the difficulty in dispersing and stabilizing particles in solvents with different re-

fractive indices, we are usually forced to apply techniques such as polymer grafting in order to enhance colloidal stability. Examples of this approach are core-shell and grafted particles which have been designed for a broad range of applications from stability and assembly, to drug delivery and carriers, films and composites, etc.[25] PS particles grafted with PEG is one example, where PEG as a hydrophilic polymer is grafted to the surface which then creates a shell with regulatory effects on stabilization. Taking advantage of adjustable shell properties, the particles can become stimuli responsive. Using PEG, or PNIPAM, as thermo-responsive shells, the structural properties of the dispersion can vary significantly with temperature, which can result in quite complex behaviour as compared with hard sphere particles being only responsive to volume fraction.[7, 26, 27] For such polymer grafts, where the corresponding polymer solutions (continuous 'free' polymers) display a Lower Critical Solution Temperature (LCST) in aqueous solutions, flocculation may be generated by an increased temperature, where monomers are attracted to each other and to the surface of other particles. As a result, the corresponding particle dispersions can display thermoresponsive properties (at high temperatures), where particles may aggregate as a result of hydrophobic interactions to further phase separate or become destabilized. Despite the fact that the LCST is a constant value, the corresponding particles may aggregate at different temperatures, i.e. at transition temperatures well below that of the free chains which can be regulated by the shell properties.[28] The grafting can be designed systematically for a specific function or application to create functional particles having desirable properties. In one particular application, we are interested in the anisotropy of particles forming linear or polymer-like structures, known as 'colloidomers'.[20] This type of assembly has been observed for non-isotropic particles. However, in case of spherical particles interacting with radially symmetric potential, studies show that particles can align linearly if a long-ranged repulsion combines with a short-ranged attractive potential.[3, 11, 15, 29–31] The strength and the range of the interactions are the parameters to vary the structural properties i.e. the thickening or branching of the backbones in the formed clusters. Such linear structures when formed have proven to be applicable in several areas, one being separation of complexes in water treatment, or film making processes. In addition, such clustering with slight tuning of the long-ranged part has found many applications in the field of protein crystallography specially in case of globular proteins whose behaviour and phase formation can be described in terms of spherical particles. The resulted clusters, however, were not completely elongated. [22] There are also applications of stripe patterns in the field of nanolithography and nanoelectricity.[32] Similar clusters (not isolated) have also been identified for particles interacting with a purely repulsive potential (repulsive shoulder) with no attractive component in the inter-particle interactions, examples of which can be core-shell particles made of dendritic, hyper-branched or diblock polymers. In this case, the strip patterns were only formed at high volume fractions and under the influence of packing mechanisms (excluded volume).[32]

One example of particles forming similar clusters in water, although challenging, is PS

particles grafted with PEG, which owing to the thermal properties of PEG can generate a short attractive potential at higher temperatures as characterized with turbidity change of the chains, or structural and dynamical changes measured by NMR or other experimental ways. For particles in water, it turns out that generating a long-range repulsion combined with such a short-ranged attraction might be challenging due to a dependence on the ionic strength and volume fraction of particles. We have made attempts to build such polymer-like clusters using a set of experimental protocols, guided by theoretical calculations. This is included in the latter chapters.

Poly ethylene glycol (PEG): PEG is a biocompatible polymer that can be found in a large variety of applications, such as drug delivery and biomedical studies, coating, etc. In general, polymers are classified according to their molecular weight (or chain length), polydispersity index (PDI), and architecture (branched, linear). PEG can be found in a large varieties of molecular weight ranging from 0.1 to 10^4 kDa. The dipole moment of PEG monomers is known to vary as it rotates, and only within a narrow angular regime, is the dipole moment high, which in turn renders the monomer hydrophilic. The population of monomers with a low dipole moment increases at high temperatures since they have a high degeneracy. Therefore, the population of hydrophobic monomers dominate at high temperatures and PEG in turn becomes hydrophobic. This is, at least, the molecular mechanisms suggested by Karlstrom[33]. Due to this behaviour, PEG has been known as a thermoresponsive polymer having an LCST close to 100 °C (for very long chains).
Poly styrene (PS): PS particles are prepared using polymerization techniques, such as emulsion and dispersion polymerization. Particles can be either hard or soft possessing gel networks which can either swell or retain their volume in a solvent. Because of feasibility and the ease of synthesis, PS often is used as a precursor for further grafting from techniques, where polymers in an additional step will be bonded to a surface.

Potential of mean force

Interactions between particles can be repulsive or attractive, depending on their nature, as well as on the properties of the surrounding solvent (if present). These forces generate a net interaction directing particles to move accordingly. By utilizing models, the net interaction free energy between particles in a colloidal dispersion can be defined, known as the potential of mean force or 'PMF'. The PMF usually amounts to a simplified, coarse-grained, description as accounting for a solvent or all atom consideration of macromolecular solutions is

often computationally demanding. The dielectric screening is an important example of solvent effects. The interactions between two charges in a gas is simply given by Coulomb's law. In a solvent, things are more complicated, and a useful approach is to average over all the interactions so that we get a form of mean interaction potential which scales with interparticle distance. This will then at large separations produce a PMF that amounts to a simple scaling of the gas phase interactions which is a simple (yet reasonably accurate) way to approximate the net interaction. We introduce further examples of PMF models in the next chapter. In the case of PS grafted with PEG, electrostatic and polymer mediated interactions are the main components of the PMF and the resulting PMF can vary with temperature, pH, etc. For instance, with a thermoresponsive shell and a good solvent, particles are assumed to remain stabilized at room temperature as a result of electrostatic and steric forces, the latter being generated by chains extending into the solvent. This results in repulsive interactions. However, a drop in the quality of the solvent at higher temperatures can change the interparticle interactions, creating a PMF which contains attractive minima. In this case, the range and the strength of the interactions can be controlled by properties of the shell. In addition to temperature, pH, ionic strength, and properties of solvent and polymer, contribute to stabilization. How to model these interactions constitute a theoretical and computational challenge. This will be further discussed in the next chapter. Polymer mediated interactions are not limited to grafted chains, and can occur in systems where polymers remain dissolved. Some polymer mediated interactions, relevant to this work, are summarized below.

Polymer structures/conformations near surfaces

Polymers form various structures near surfaces. Partially adsorbed chains in a good solvent can be characterized by three main parts as illustrated in figure 1.1 (left panel). Parts of the segments are bound to form 'train' conformations, whereas the unbound ones connected to trains form loops, and the non-adsorbed terminals are the tail parts of the chains. Grafted chains (in a good solvent) are categorized differently. Being a function of polymer

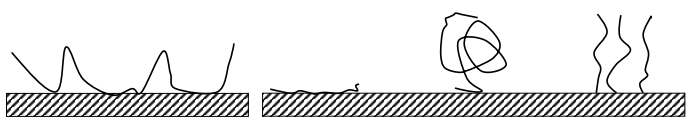

Figure 1.1: Polymer conformations near surfaces. The graph to the left describes the chains with partial adsorption whereas the right figure demonstrates the structures of the grafted chains at surfaces.

concentration, monomer-surface interactions, as well as chain flexibility, three main conformation regimes are known to form. If the monomers have tendency to attract to the surface, polymer chains, at low concentrations, tend to smooth out on the surface to form

a pancake conformation. As the concentration increases, due to a larger number of chains and inaccessibility of surface, polymer chains form mushroom conformations. Increasing the concentration further, chains extend out to minimize their contact with neighbours forming brush shape conformations.

Polymer mediated interactions

Depending on the surface affinity of the polymer, surfaces covered with polymers can generate repulsive or attractive forces between the surfaces. The interactions between particles covered with polymers can also be repulsive or attractive. For polymers with a radius of gyration far less than the particle size, where Derjaguin's approximation (DA) is valid, the particle surface can be modelled by planar surfaces. The DA is explained in the next chapter. For small particles and long polymers, polymers can mediate many-body interactions. The mechanisms for interactions in the former case are illustrated in figure 1.2.

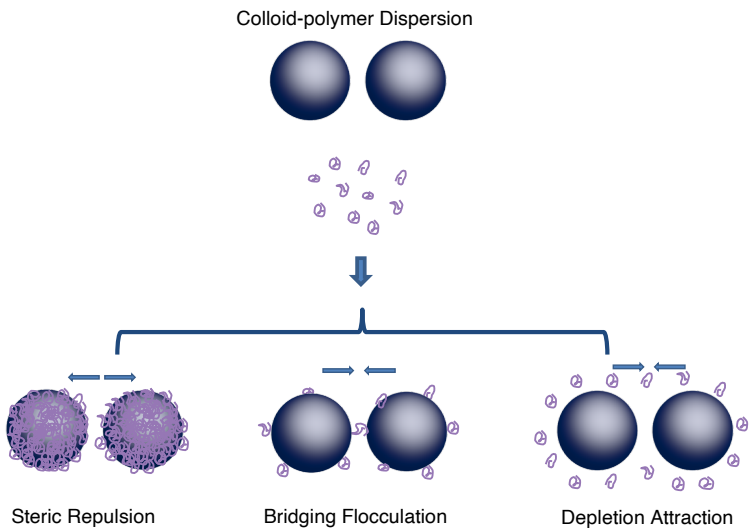

Figure 1.2: Polymer-mediated interactions in colloid/polymer dispersions.The mechanisms differ depending on whether non-adsorbing or adsorbing polymers are added.

In such systems, as evident, similar mechanisms may occur between particles as compared with planar surfaces, in the presence of polymers, allowing for a controlled stability. Let us, for now, limit the discussion to particles in the presence of polymer dispersed in a good solvent. In the case of non-adsorbing polymers, the resulting interactions between two proximal particles are attractive. This is attributed to a decrease in the osmotic pressure of the added polymers in the interparticle regions, which stems from the unfavourable en-

tropic loss that polymers experience due to the limited chain conformations in this region. This results in polymers being depleted from the region (depletion region) and a resulting entropy driven force causing particles to aggregate in order to reach a minimum free energy. The effect is known as depletion attraction. Although non-adsorbing polymers cause destabilization of colloidal dispersions in most cases, within certain regime of polymer concentration, they can also provide some degree of stability. This happens when an increased viscosity of dispersant because of polymer addition slows down the movements. But this only affects kinetics, not the final equilibrium (although complete equilibrium might not be reached in practice). This is also considered as an arrested dynamics. Particle move slowly in a low concentration regime until depletion interactions starts to dominate. Short polymers may contribute to slower dynamics, rather than inducing depletion interactions. This trend is opposite for cases where long polymer chains are used.
The range of the depletion attraction has been estimated as $2Rg$, where Rg is the radius of gyration of polymer chains.[30, 31, 34] This estimate is not exact but it can be used under certain conditions, in dilute polymer solutions. (reasonable also at higher concentration in theta-solvents)
For adsorbing polymers, approaching particles may experience different forces, attractive or repulsive, depending on the polymer coverage and monomer-monomer as well as monomer-surface interactions. Small polymer adsorptions result in polymer bridging over surfaces whereas stronger adsorptions can generate steric forces, at least due to the non-equilibrium effects, (see below). The former causes adsorption or bridging flocculation whereas the latter results in repelling interactions. The steric forces are entropic driven due to the compression of polymer chains when particles approach. This would be under the assumptions that the monomers do not attract each other, i.e. in a condition that particles are dispersed in a good solvent which results in chains extending outward in the solvent. It should be noted that in such systems, non-equilibrium effects often influence the interactions between polymer-adsorbing surfaces or particles. The reason can be associated to the slow diffusion specially for long chains which tend to attach to surfaces almost irreversibly. [35]

Polymer mediated interactions may change under the influence of solvent quality. This can be caused by a temperature variation, in case of thermoresponsive polymers, inducing hydrophobic interactions which can dominate at higher temperatures, inducing particle aggregation. Interactions in a system containing hydrophobic particles, and non-adsorbing polymer, can be altered by a temperature change, dividing to regimes where depletion or bridging interaction dominate. One might expect that the interactions remain attractive with increasing temperature, going from depletion to bridging regimes. However, in a work by Xie et al, a non-monotonic response of aggregation upon a temperature increase was noticed.[36, 37] The intermediate regime was observed to be dominant by strong repulsions resulting in a redispersion of the particles. In contrast to the above mentioned illustration, the type of polymer mediated interactions generated were repulsive, albeit in

a less good solvent.[36] The reason was associated to the change in the pressure generated from the polymer induced interactions upon a transition from depletion to bridging. This work was purely theoretical and utilized a density functional theory (DFT) model, suggesting such re-entrant behaviour even in the absence of electrostatic interactions, i.e. only due to the polymer mediated interactions. No experimental analysis was reported in their work. In an earlier study, Feng et al established such behaviour experimentally, arriving at similar re-entrant properties.[38] The prerequisite for observing such behaviour seems to be that solvophobic particles and a non-adsorbing polymer showing an LCST are used for analysis. In the next work, using a combination of theory and experiment, we tried to investigate such non-monotonic temperature response of polymer-mediated interactions in dispersions containing grafted particles in the presence of a dissolved polymer, which is chemically identical to the polymer grafts. The results are summarized in later chapters.
The stabilization of particle/polymer dispersions can also be influenced by parameters such as pH, ionic strength, temperature, etc. In case of a thermoresponsive polymer, such as PEG, the resulting interactions can vary dramatically with temperature. Similarly, for polyelectrolytes, the interactions can be regulated by changing the ionic strength, or pH, which in turn govern the net charges, and the range of the electrostatic interactions. Polymer-mediated interactions are still subject of many studies due to the wide range of applications that they offer. Just to mention few examples, dispersions containing particles and polymers can be used as precursors for modifying the interfacial chemistry. Examples of applications include the use of lubricant agents to change the flow properties when binding or adsorbing to surfaces, or for purification and extraction of compounds in water treatment when complexes are formed and removed, for dispersal of drugs in drug delivery, etc.

1.2 Capillary induced phase transition

Polymer solutions may behave differently in the presence or in the absence of surfaces. The differences may include changes in kinetic response, thermodynamic properties, etc. We devote the next part of this thesis to the phase study of polymer solutions showing LCST, under the effect of surfaces or capillaries. Therefore, we first give a short introduction on phase equilibria of polymers in bulk solution. Next, the effect of confining surfaces, such as capillaries, will be discussed. We chose to study dispersions of PNIPAM and silica in our experimental work, which we summarize below.

PNIPAM is another example of a thermo-responsive polymer, showing an LCST at around 32 °C. Due to its low transition temperature, which is close to our body temperature, PNIPAM has been widely used for biomedical studies. PNIPAM also exists in various ranges of molecular weight, and is sometimes synthesized with functional groups.
Silica can exist in many forms, wafer/film or particle, porous and non-porous. Silica can be synthesized using the Stober technique, where colloidal particles in a form of sol-gel suspension can be prepared or precipitated. Silica is also formed from a reaction of sodium silicate in alkaline condition, yielding white silica powder.[39] The porous or mesoporous silica is another form, which is produced using a modified Stober technique. [40]The surface of silica is mainly composed of $Si-O-Si$ (siloxane) and $Si-OH$ (silanol) groups, with the former turning to $Si-OH$ when pH of the solution changes. Owning to its properties, silica can be used for regulatory studies, such as hydrophobicity change of surfaces, using pH. There are several forms of silanol groups, varying in structure and the number of OH groups (or pKa). The most stable forms of silanol are known as external geminal and internal geminal, with their corresponding pKa of 3 and 9.[41] Silica surfaces become hydrophilic, at pH values above these pKa values, which is associated with the higher charge density (negative), as a result of the surfaces being deprotonated. At a lower pH, the particles carry weak negative charges, whereby the surface is less hydrophilic. The surface charge of silica thus varies with pH. The isoelectric point of silica, where surface carries no net charges, is at $pH = 2$. Because of the pH regulation, the change in surface property using ionic strength formulation/salt addition is possible, whereby electrostatic interactions are adjusted, using both pH and salt concentration. This results in a dual surface response. Another advantage of using silica is the ease of functionalization, where dry/wet modification techniques are used to change the surface properties. For instance, polymer grafting using various types of silane agent have been used to create hydrophobic or hydrophilic surfaces, depending on the number of silane groups, and their types. The importance of using a silica as a surface active material can be specially highlighted for biomedical and drug delivery studies for thermo or pH-regulatory properties.[41, 42]

Thermodynamics of polymer solutions

The thermodynamics of solubility can be described in terms of the free energy given as,

$$\Delta G = \Delta H - T\Delta S \tag{1.1}$$

where the first term in the right side of equation defines the enthalpy contribution and the second term accounts for the entropic effects. The free energy change of molecules into a solvent, ΔG, is therefore composed of an enthalpy and an entropy change, ΔH and ΔS. For very dilute solutions, the free energy drop is entropy-driven, independent of the interactions. Whether or not having a spontaneous solvation is related to these terms yielding a negative value for the free energy. For polymer chains in solvent, the entropic loss due to the translational constraints is the main reason for the reduced solubility as compared to the monomers in the solvent. However, the total energy term between monomers and solvent remain unchanged. In general, using Flory-Huggins (FH) theory and/or DFT, the phase diagrams of polymer solutions are investigated. The FH does not include the effect from surfaces (if existing) and in many cases, DFT is used for this purpose. However, the (Schentjens-Fleer) theory is an alternative approach, which is closely related to FH. Both theories can qualitatively predict the phase responses of polymer solutions. Here, we describe the FH for polymer solutions, and in the next chapter we explain the Density Functional Theory (DFT) in a general form, with an extension to consider the effect from surfaces. In the following, FH is explained for a polymer/solvent solution. A lattice of N cells is occupied by N_1 solvent molecules and N_2 polymers of length r (or rN_2 monomers), ($N = N_1 + rN_2$) giving rise to a free energy of solvation:

$$\Delta H = kTN_1 v_2 \chi(T) \tag{1.2}$$

$$\Delta S = kT(N_1 lnv_1 + N_2 lnv_2) \tag{1.3}$$

$$\Delta G = kT(N_1 lnv_1 + N_2 lnv_2 + N_1 v_2 \chi(T)) \tag{1.4}$$

$$\chi(T) = \beta z \Delta\epsilon_m \tag{1.5}$$

$$\Delta\epsilon_m = \epsilon_{12} - \frac{\epsilon_{11} + \epsilon_{22}}{2} \tag{1.6}$$

where χ is the Flory-Huggins parameter, $\beta = 1/kT$ the inverse thermal energy, z is the number of neighbouring elements and ϵ is the interaction parameter between 'segments' (i.e. the solvent molecules or monomers). Interactions are limited to the nearest neighbours (z). Dividing eq. 1.4 by ($N_1 + rN_2$),

$$\Delta g = kT(v_1 lnv_1 + \frac{v_2}{r} lnv_2 + v_1 v_2 \chi(T)) \tag{1.7}$$

v_1 is the volume fraction of solvent and v_2 is the volume fraction of polymer: $v_1 = \frac{(N_1)}{(N_1+rN_2)}$ and $v_2 = \frac{(rN_2)}{(N_1+rN_2)}$. The chemical potentials and the spinodal curve, satisfying $\frac{\delta^2 g}{\delta {v_2}^2} = 0$, can be calculated as follows,

$$\beta\Delta\mu_1 = \beta\frac{\delta}{\delta N_1}(\Delta G) = lnv_1 + v_2(1 - 1/r) + {v_2}^2\chi(T) \tag{1.8}$$

$$\beta\Delta\mu_2 = lnv_2 - rv_1(1 - 1/r) + r{v_1}^2\chi(T) \tag{1.9}$$

$$v_2 = \frac{1}{2}(1 - \frac{r-1}{2-\chi} \pm \left[(1 - \frac{r-1}{2r\chi})^2 - \frac{2}{\chi r}\right]^{1/2}) \tag{1.10}$$

The points on the spinodal curve are collected by finding the inflection points of the free energy curve, at each temperature, which results in a $T - v_2$ curve where v_2 then marks the limit of the solubility ($\chi \propto T$). These points are in fact the cloud points of solutions where phase transition (often coil-globular) occurs, depending on the temperature and the volume fraction of polymer. The standard FH can only suggest a $\cap$-shape curve but never a $\cup$-curve. For aqueous PNIPAM/PEG solutions, the phase diagram form a well-known U-shape curve with its minimum being the LCST. The assumption made in FH is that the mixture is incompressible and the volume of the cells in the lattice remain unchanged. The FH has been modified in many ways to include the effects from compressibility, and degeneracy of monomer states.[33] For instance, in a work by Karlstrom[33], the effects from monomer degeneracy has been accounted for which is a more appropriate form when dealing with a phase diagram of PEG/water, where the monomers can be more or less hydrophilic, depending on the internal structure (angles) of the monomers. The FH has also been extended to include the effects of added particles on the phase transitions of a polymer solution. [43] The result was a polymer solution generating CIPS (capillary induced phase separation) which was accounted for by an additional 'surface effect' term. Particles were dispersed in solutions of adsorbing polymer and their effect was attributed to CIPS rather than depletion or bridging effects.[43] The CIPS effect will be explained in the following section.

CIPS

Phase transitions of dispersions are known to be influenced by the presence of surfaces. In case of simple molecules, for instance water molecules in form vapour close to hydrophilic surfaces, condensation has been characterized by an early surface wetting. In this case, the

driving force for condensation is associated with the surface affinity in combination with attractive intermolecular interactions in water. Vapor-liquid coexistence is the equilibrium state under this circumstance. Example of a one-component system can be vapour of nitrogen confined in porous medium, where a type fourth (*IV*) adsorption isotherm (adsorbed amount against vapour pressure) is attributed to a capillary condensation, forming rapidly at higher temperatures (still below T_c). [44, 45] Similar observations can occur in a dispersion of oil (apolar medium) and dissolved water close to hydrophilic surfaces forming liquid-liquid phases at equilibrium. These results are not limited to flat surfaces and may affect the properties of dispersions in capillaries, and capillary induced phase transition (CIPS) may take place under certain conditions. CIPS can also occur in solutions containing adsorbing polymers, where phases rich and poor in polymer concentration are the coexisting phases at equilibrium. The reason is associated to the tendency of polymers to adsorb at the surfaces. Effects from pH, temperature, ionic strength, etc may also affect the CIPS response. [43, 46–48]

Beside experiments, there are also theoretical models of CIPS introduced under supracritical conditions. In a work by Xie et al, the model was established using a DFT approach, suggesting a shift to the LCST, caused by capillary effects.[49, 50] The size of the pores was found to be a crucial parameter for observing the CIPS effect. The experimental verification of the model, however, was left for future analysis. An advantage of using DFT is that, being a free energy functional, we can directly relate the phase behaviour in pores to the corresponding phase diagram in the surrounding bulk. There is another relevant case of an 'early' phase transition due to CIPS which has been noticed in studies of PCMs (phase change materials) confined to porous medium. The characteristic phase transition temperatures (T_g, T_m), in the presence of capillaries, occurred below that of the bulk solution (polymer melt), due to surface effects. The size of pores (mesopores) and the PCM composition were found to be important parameters varying the transition temperature. [44, 51, 52] In the last work of this thesis, we tried to experimentally verify our theoretical results of a capillary LCST which is lower than in the bulk. Phase transitions of polymer solutions with and without the presence of surfaces can be characterized by techniques such as NMR[1] [53] as well as rheometry. Using NMR, the mobility and conformational change of polymer chains can be detected from an NMR spectrum, where different conformations with their respective chemical shifts can be measured, as an indication of phase transition. A varying viscosity in rheometry experiments can also be used for detection of aggregation. The capillary force between surfaces can generate repulsive or attractive interactions. However, if a phase separation occurs in the form of CIPS, the force is long-ranged, and attractive in nature. Experimentally, the force can be measured using the surface force apparatus, SFA, where the interaction at compression/separation can be obtained as a function of distance.[54] As mentioned, the interactions between surfaces covered with polymer are often influenced by non-equilibrium effects, where the chains need to relax and diffuse for

[1]NMR: acronym, explained on the next pages

long enough time to display equilibrium properties. Due to this reason, the separation curve almost never coincides with the curve found for approaching surfaces. Despite the success in the measurement of the interactions using experimental techniques, the compositions of phases are often challenging to be measured directly. In theory, however, the density distribution and compositions of phases have been obtained from simulations and using theoretical tools such as DFT. We will study CIPS and bulk phase transitions using DFT, which will be discussed in the next chapter.

Chapter 2

Theory

Why do we use simulations? Simulations may generate a deep understanding of systems especially at small scales, such as the atomistic level, where experimental approaches are not always accessible or easy tasks for studying and analysing system properties. By using simulations, effects of many parameters on behavioural changes can be made possible. We also need a suitable model in order to set up the simulation. This can be achieved by applying approximate tools, such as DFT, which can be powerful and versatile for studies on more complex systems such as polymer/particle dispersions. We will introduce molecular interactions at small scales, as well as generic models of interactions (such as Potential of Mean Forces, PMFs), with the aim to describe systems and predict their macroscopic behaviours. We then proceed to explain a DFT-established PMF for modelling and analysing polymer/particle dispersions. Finally, we describe Metropolis Monte Carlo simulations, to which the established model PMFs are imported, and properties at equilibrium are obtained.

2.1 Statistical mechanics

Statistical Mechanics is a tool for relating macroscopic properties of a system to its microstates' properties. When investigating equilibrium properties, we often refer to Statistical Thermodynamics. In this context, we are dealing with systems with small volumes and dimensions at atomic levels. We therefore need to first simulate the model systems and calculate probability distributions of desired properties. One crucial concept here is an 'ensemble', which is a mental construction of a large number of macroscopic subsystems having the same thermodynamic properties, but varying in the microstate/molecular level. The value of a mechanical variable can then be calculated by averaging over these micro-

states. By mechanical variable, we mean parameters such as pressure, volume, energy, and number of particles, that can be defined for a single microstate configuration. A known postulate (ergodic hypothesis) is that at equilibrium, the ensemble average and the time average of a mechanical property, are equivalent. The ensemble average is used to report the thermodynamic properties of the system we investigate. The following expression is the result of this hypothesis:

$$< f >= \int f(\vec{p},\vec{r})\rho(\vec{p},\vec{r})d\vec{p}d\vec{r} = \lim_{\tau\to\infty} 1/\tau \int_0^\tau f(t)dt \tag{2.1}$$

where τ is the duration of an experiment and $\rho(\vec{p},\vec{r})$ is the probability of observing a microstate having momentum p and position r. The brackets indicate an ensemble average, and f is a mechanical variable.

To reproduce a real system, the probability of each microstate must be known, which is performed by weighting in terms of a suitable Boltzmann factor, i.e. the configurations are Boltzmann weighted. If we consider a canonical ensemble (N,V,T) in thermal equilibrium with a heat bath with temperature T, then each microstate consists of N molecules with volume of V. The partition function, Q, in this ensemble in the classical description, can be written as:

$$Q = \frac{1}{h^{3N}N!}\int\int e^{-\beta(K+U)}d\bar{r}^N d\bar{p}^N \equiv Q_{trans}\frac{1}{N!}\int_V e^{-\beta U(r^N)}d\bar{r}^N \tag{2.2}$$

where h is the Planck's constant, K and U are kinetic and potential energy, respectively, $\bar{p}$ is the momentum and $\bar{r}^N$ represents the coordinates of N molecules, while β=1/kT is the inverse thermal energy with k being Boltzmann's constant. The term 'partition function' in Statistical Mechanics is based on the partitioning of energy between all the members of an ensemble (with their associated energies) using Boltzmann weighting, from which macroscopic/thermodynamic properties, such as pressure can be estimated.
By integrating out the kinetic term, we find the translational part of the partition function as an independent factor, Q_{trans}. The configurational partition function is denoted Q_c. Q_{trans} and Q_c are given as,

$$Q_{trans} = \frac{1}{h^{3N}}(2\pi m k_B T)^{3N/2} \tag{2.3}$$

$$Q_c = \frac{1}{N!}\int_V e^{-\beta U(r^N)}dr^N \tag{2.4}$$

The full classical partition function is written as,

$$Q = Q_{trans} Q_c \tag{2.5}$$

The Helmholtz free energy in a canonical system can be obtained from the partition function given as,

$$A = -k_B T ln Q_{N,V,T} \tag{2.6}$$

We note that we do not (normally) establish Q itself, but rather an average mechanical property, $\langle X \rangle$. For instance the energy, U, can be calculated as,

$$\langle X \rangle = \int \frac{dr^N exp\left[-\beta U(r^N)\right] X(r^N)}{\int dr^N exp\left[-\beta U(r^N)\right]} \tag{2.7}$$

The value written in the denominator is the configurational part of the partition function, Q_c (except for the factorial term). In order to establish this average, we need to make some assumptions, such as pair-wise additivity of interactions for finding the total energy potential, $U(r^N)$, and choose a suitable numerical approach, which will be explained further below.[55, 56]
There are also NPT (isothermal-isobaric) and μVT (grand canonical) ensembles, through which similar thermodynamic properties of systems can be obtained, but with different macroscopic constraints, such as constant NPT and constant μVT. μ is the chemical potential.[55]

2.2 Intermolecular interactions

If we consider an ideal gas, i.e. (essentially) non-interacting particles, the free energy and other properties of the system can be calculated exactly. If we, however, choose any other system, as a more realistic one, we have to deal with correlations, and many types of interactions. Such interactions can be categorized as: attractive/repulsive, short-ranged/long-ranged, strong/weak and isotropic/directional. Also, they can be classified as electrostatic/non-electrostatic, depending on their physical and chemical origin. Analytical models, often semi-empirical, are usually based on assumptions such as pair-wise additivity which reduce the model complexity. More advanced treatments can be applied to account for many-body effects. However, in the systems we study here we neglect such higher order interactions. Therefore, we use the term 'pair potential' to describe the interactions between particles, whereas U denotes the sum over all such pair interactions. The models have both

advantages and disadvantages, and while one might reproduce a certain property correctly, one might fail to capture other properties. The models therefore vary in simplicity and accuracy. The Coulomb interaction, for instance, is characterized as a long-ranged potential. The van der Waals (vdW) originates from Keesom, Debye and London (dispersion) interactions, which compared to Coulomb, are short-ranged ($\propto 1/r^6$). The strength of these potentials can be described in terms of the thermal energy (kT). More examples of simple model potentials, known as generic potentials, are summarized below.

The Mie potential is a semi-empirical pair potential which consists of attractive and repulsive parts. The Mie potential is defined as,

$$u(r) = -B/r^j + C/r^j \tag{2.8}$$

Where B and C are the potential constants. The negative term measures attractive interactions whereas the positive part describes the repulsive forces. The special case of the Mie potential is the well-known Lennard Jones (LJ) potential with (6,12) as exponents.

Lennard Jones or L-J potential: The interaction potential contains both a repulsive (at short range) and an attractive term (at long range). In this case, the short ranged potential describes the Pauli-repulsion interactions which occurs when electron clouds overlap, whereas the attraction originates from vdW interactions:

$$u(r) = 4\varepsilon \left[(\frac{\sigma}{r})^{12} - (\frac{\sigma}{r})^6 \right] \tag{2.9}$$

where ε is the depth of the attractive well. The potential is zero at $r = \sigma$, approximately a distance equal to one particle diameter.

Hard-sphere potential: The interactions are non-zero and repulsive only when particles are in contact. The pair potential is written as below. It is often used to model the Pauli repulsion at short range,

$$u(r) = \begin{cases} \infty & , r < \sigma \\ 0 & , r > \sigma \end{cases} \tag{2.10}$$

The hard sphere potential is also often used to describe the steric repulsive interactions between surfaces grafted with polymer, where surfaces cannot approach further due to the incompressibility of the polymer layers.

The Morse potential: The Morse potential can be used to describe attractive intra- and inter-molecular interactions.

$$u(r) = Z[(1 - e^{-b(r-r_e)})^2 - 1] \tag{2.11}$$

where Z is an energy scaling factor to set the magnitude/strength of the potential, r_e is the position of the minimum, whereas b regulates the range of the interaction (small b $\Rightarrow$ wide 'well'). [56]

2.3 Potential of mean force

In the previous chapter, we defined the PMF as a mean potential between particles that accounts for all the interactions from implicitly treated molecules/particles. For instance, the Coulomb interaction between two ions in vacuum effectively becomes weaker in a solvent. This is often approximated via a single scaling, by $1/\varepsilon$, of the Coulomb interaction in vacuum. The general definition of PMF as an effective potential, w(r), between two particles, separated by r, immersed in an N-particle system, where these N particles are treated implicitly, is given below,

$$w(r) = -kTln[\int d\overline{R}^N exp(-\beta U_{tot}(r, \overline{R}^N))] + s \tag{2.12}$$

where U_{tot} is the sum of all the pair-wise interactions. The s, constant term, is usually chosen so that $w(r \to \infty) = 0$. An example of a model PMF is the depletion interaction. If we consider two spherical particles with radius R, immersed in a solution containing non-adsorbing polymers, we can arrive at an approximate depletion PMF, W_{dep}, by stipulating a depletion thickness δ, and an overlap volume, V_{ov}:

$$W_{dep}(h) = \begin{cases} \infty, & h < 0 \\ -\Pi V_{ov}(h), & 0 \leq h \leq 2\delta \\ 0, & h \geq 2\delta \end{cases} \tag{2.13}$$

where h is the surface distance and Π osmotic pressure. With a point-like monomer model approximation (for theta solvent, ideal chains) and a model where polymers are described as freely overlapping spheres, Π and V_{ov} are given as,

$$V_{ov}(h) = \frac{\Pi}{6}(2\delta - h)^2(3R + 2\delta + h/2) \tag{2.14}$$

$$\Pi = n_p^{free} kT \tag{2.15}$$

where n_p^{free} is the number density of polymer chains, (equal to n/v_f, n number of chains divided by v_f, the free volume). The free volume is the accessible volume for polymer chains, subtracting the volume occupied by particles and the depletion zones. The thickness of the depletion layer is often estimated as the radius of gyration of polymer, R_g, but in a good solvent, this value decreases at high polymer concentrations. [57]

2.4 Colloidal stability

Due to the large size of particles which can cause aggregation, controlling the stability of particles is often difficult. The stability range is often described in terms of a parameter known as the sedimentation length, L, at which the opposing forces against particle thermal movements, such as gravitational forces becomes dominant,

$$L = \frac{kT}{\frac{4}{3}\pi R^3 \Delta\rho g} \tag{2.16}$$

where R is the radius of particles, $\Delta\rho$ is the difference in the density of particle and solvent, and g is the gravitational acceleration. For $L > R$, particles remain stable in solution without sedimentation. In colloidal dispersions, with the particle size ranging from 10 nm to 1 μm, the thermal energy usually overcomes the gravitational force causing particles to move randomly. These random movements, which are as a result of collisions with solvent molecules, are known as Brownian motions. As particles become larger, the attraction due to the van der Waals forces can be dominating, which can then cause particle aggregation. The vdW pair-interactions which separately decay as $1/r^6$, leads to a complete PMF with a more long-ranged dependence. The vdW interaction, W(r), between two particles with radius R, separated surface distance r, can, at large distances compared to the size of particles, be written as,

$$W(r) = -\frac{H}{6}\left[\frac{2R^2}{r^2 - 4R^2} + \frac{2R^2}{r^2} + ln\left(1 - \frac{4R^2}{r^2}\right)\right] \tag{2.17}$$

where H is the Hamaker constant. The interaction (W) between planar surfaces/ particles simplifies at small distances (h):

$$W(h) = -\frac{H}{12\pi h^2}, (planes, J/m^2) \tag{2.18}$$

$$W(h) = -\frac{H}{12h}R, (particles, J) \tag{2.19}$$

To counteract these attractive forces, refractive index matching is often utilised by choosing a proper solvent. Other options include stabilization techniques, such as polymer grafting or charging.[13–16] In addition to vdW interactions, the electrostatic potential generated from the surface charges must, in the latter case, also be taken into account. The charges can either originate from the material itself, or are obtained from the adsorption from surfactants/ions. If we consider interactions between charged ions confined in a planar geometry, or between two colloidal particles (with a size considerably larger than the separation), the forces between positive and negative charges create a diffuse layer of ions and

counter-ions surrounding the colloids, known as the electrostatic (ES) double layer (DL). The first layer of counter ions is bound tightly to the surface whereas ions in the next layer are more mobile. Addition of salt will effectively screen the ES interactions between charged colloidal particles causing a reduction of the double layer. The overlapping double layers in a dispersion of colloidal particles will then produce an effective repulsive potential, which is often modelled by a mean field approximation (valid under certain conditions). For charged particles, the total interaction potential between particles is often modelled based on DLVO (Derjaguin, Landau, Vervey, and Overbeek) theory, which utilizes a superposition of an electrostatic double layer repulsion and attractive vdW interactions as an interaction free energy. The DLVO theory often provides a good approximation for colloidal stability, and interactions between charged colloidal particles.[27, 58–61] Specifically, the interaction free energy per surface is estimated as, [58]

$$W(h) = W_{dl}(h) + W_{vdW}(h) \tag{2.20}$$

$$W(h) = \left(\frac{Z_{eff}}{1+\kappa R}\right)^2 \frac{l_B k T}{r} exp(-\kappa(r-2R)) - \frac{H}{12h}R \tag{2.21}$$

Where r is the center-center distance between the particles, κ, is the inverse of Debye length, and R is the size of the particles. The l_B is the Bjerrum length with its value being 0.7 nm in water. The number of surface charges is in this model, assumed to be constant. κ is defined as,

$$\kappa^{-1} = (\frac{k_B T \varepsilon_0 \varepsilon}{2e^2 N_A I})^{1/2} = \frac{0.3\ nm}{I^{1/2}} \tag{2.22}$$

where e is the elementary charge, N_A is the Avogadro's number and I is the ionic strength which is calculated by,

$$I = \frac{1}{2}\sum_{i=1} z_i^2 c_i \tag{2.23}$$

z_i is valency of ion type i and its concentration, c_i. The Debye screening length is a measure of the thickness of the DL layer. The strength of the DL forces is dependent on the effective surface charges, Z_{eff}, the salt concentration, c_i, and the dielectric constant of solvent, ε. The double layer free energy is often accurate at large separations and low surface charges. At high surface charge densities, the non-linear Poisson-Boltzmann (PB) theory is often used[58]. However, in the presence of multivalent salt even the full Poisson-Boltzmann may not be able to suggest correct behaviours, even qualitatively. The PB equation is given

as,

$$-\epsilon_0\epsilon_r \bigtriangledown^2 \Phi(z) = e\Sigma_i z_i c_0 exp(\frac{-z_i e\Phi}{kT}) = e\Sigma_i z_i c_0 - e\Sigma_i(\frac{z_i^2 c_0 e\Phi}{kT}) \tag{2.24}$$

Where Φ is the electrostatic potential. The first equality represents the non-linear PB whereas the last term is the linearized form of the differential equation. Note that $\Sigma_i z_i c_0 = 0$ due to electroneutrality. The linearized form of the PB potential known as Debye-Huckel, is given below,

$$\Phi = \frac{ze}{4\pi\epsilon_0\epsilon_r} \frac{exp(-\kappa(r - R_{ion}))}{r(1 + \kappa R_{ion})} \tag{2.25}$$

In cases where there are additional interactions involved, such as hydrophobic or steric potentials, the DLVO theory needs more modifications, taking into account effects such as grafting density or temperature controlled interactions. In general, DLVO is considered as an accurate model of weakly charged particles and monovalent salts. However, in this work, a DFT model will be used to treat interactions due to a grafted layer and temperature controlled polymer-mediated interactions. (Note: there are also non-grafted polymers.)

We note that we do not address the kinetic issues here, as it is beyond of the scope of this thesis, except to some extent in our work on linear structures, some of which are metastable. In this context, we can mention more general terms such as aggregation regimes and particle diffusion. Generally, aggregation occurs in three regimes, early and late stages, and final sedimentation stage. The aggregation is either diffusion or reaction controlled. The former occurs fast, and the latter is slow aggregation, being dependent on the barrier height of the energy potential. Particle stability can then be kinetically controlled, by adjusting parameters such as temperature, viscosity and the free energy barriers.[62]

Another important phenomenon is particle transport. The ballistic and diffusive motions are the two regimes of motions at microscopic scales. In a ballistic regime, particles can travel lengths larger than the particle size, without any collisions with other molecules. However, in a diffusive regime, which is relevant for colloidal systems, a particle's motion is disturbed by collisions with other particles. The diffusive motion is slower than the ballistic motion. In the diffusive regime, the diffusion coefficient of particles moving can be obtained from the Stokes-Einstein relation which is inversely proportional to the hydrodynamic radius of the particles. This will be discussed further in the later chapter.

2.5 Density functional theory

The classical Density Functional Theory, or DFT, is a powerful technique based on free energy minimization to obtain properties at equilibrium conditions, such as density profile and PMFs. The DFT can be used with good accuracy for polymer solutions in heterogeneous environments. We use the theory established by Woodward [63], sometimes with an extension to semi-flexible chains in order to investigate polymer-mediated interactions. All polymer configurations are accounted for, in a coarse-grained manner, subject to a mean field Boltzmann weight. For a system with symmetry allowing 1D- and 2D-dependent densities, as obtained by mean-field integrations, the DFT can be extremely efficient. We shall first start with the DFT model for a heterogeneous dispersion of simple particles, where the configurational free energy functional can be derived from 'the canonical integral' from which the equilibrium density profile of particles, n($\bar{r}$), can be obtained. We note that as the kinetic partition function is constant, we can exclude it from the equations. For a system outside a flat surface (say), the (x,y) dependence can be integrated out via a mean-field approximation. This leaves us with z-dependent quantities.

$$A_c[n(z)] = k_B T \int_V dz n(z)(ln[\frac{n(z)}{\chi_F}] - 1) + \frac{1}{2}\int_V dz n(z) \int_{V'} dz' n(z')\phi_s(|z - z'|) + \int_V dz n(z) V_{ext}(z) \tag{2.26}$$

where A_c is the Helmholtz free energy for the configurational part, V is the volume (integral from a surface (at $z = 0$) and outwards $\int_0^\infty dz$), V' is the volume outside hard sphere of particle at z, ϕ_s is the interaction potential between particles positioned at z and z' (accounting for non-locality of particle-particle interaction), V_{ext} is the external potential from the surface, and χ_F, is the free volume fraction, which can be estimated as $1 - \sigma^3\overline{n}(\overline{z})$ for a coarse grained calculation [1], where the non-local excluded volume is accounted for. The first integral calculates the free energy of the solution including the entropic effects related to the excluded volume, the second integral is taking into account the interactions between fluid particles and the last term is for calculating the contribution from the external potential on the solution which is the main reason for observing a non-uniform particle distribution. [56]

Let us now assume that we are interested in finding the free energy cost of moving $\delta N =$

[1] χ_F=1 $- \sigma^3\overline{n}(\overline{z})$ for a fine-grained model, $\overline{n}$ being the coarse-grained density, averaged over a volume surrounding the particle at $\overline{z}$

$\int_V n(\bar{r})d\bar{r}$ molecules from the bulk. The grand potential is then obtained as,

$$\Omega[n(z)] = A[n(z)] - \mu \int n(z)dz \tag{2.27}$$

Given the grand potential, we can find the most probable density distribution by minimizing the free energy, $\frac{\delta\Omega}{\delta n}(z) = 0$. The density distribution of particles for an ideal solution, i.e. when the particles do not interact ($\phi = 0$) is then obtained as follows,

$$n(z) = e^{\beta\mu}.e^{-\beta V_{ext}(z)} = n_{bulk}e^{-\beta V_{ext}(z)} \tag{2.28}$$

polymer-DFT

Including more complexity in the model, the effects from bond potentials must be considered. For example, the presence of a polymer, whether adsorbing or non-adsorbing to the surfaces, influences the interactions. For ideal polymer chains (r-mers), the density profile can be calculated from the equations below. We let $\overline{R} = (\bar{r}_1, \bar{r}_2, \cdots, \bar{r}_r)$ denote a configuration where monomers are at $\bar{r}_1$, $\bar{r}_2$, $\bar{r}_3$, etc., so that $N(\overline{R})d\overline{R}$, is the number of chains with configurations between $\overline{R}$ and $\overline{R} + d\overline{R}$. Then,

$$\beta\Omega_{eq} = \int N_{eq}(\overline{R})(ln[N_{eq}(\overline{R})] - 1)d\overline{R} + \beta \int N_{eq}(\overline{R})(V_b(\overline{R}) + V_{ext}(\overline{R}) - \mu)d\overline{R} \tag{2.29}$$

V_b is the bond potential between neighbouring monomers along the chains. The density distribution of polymer at equilibrium, N_{eq}, that minimizes the grand potential, takes the form,

$$N_{eq}(\overline{R}) = e^{\beta\mu}.e^{-\beta V_{ext}(\overline{R})}.e^{-\beta V_b(\overline{R})} \tag{2.30}$$

The bond potential can be written as,

$$V_b(\overline{R}) = \sum_{i=1}^{r-1} V_b(|\bar{r}_{i+1} - \bar{r}_i|) \tag{2.31}$$

The external potential acts on each monomer:

$$V_{ext}(\overline{R}) = \sum_{i=1}^{r} V_{ext}(\bar{r}_i) \tag{2.32}$$

Hence:

$$N_{eq}(\overline{R}) = e^{\beta\mu}.e^{-\beta\sum_{i=1}^{r} V_{ext}(\bar{r}_i)}.e^{-\beta\sum_{i=1}^{r-1} V_b(|\bar{r}_{i+1}-\bar{r}_i|)} \tag{2.33}$$

The density distribution of monomers, $n_{eq}(\bar{r})$, is obtained as follows,

$$n_{eq}(\bar{r}) = \int \sum_{b=1}^{r} \delta(\bar{r} - \overline{r_b}) N_{eq}(\overline{R}) d\overline{R} \tag{2.34}$$

Or:

$$n_{eq}(\bar{r}) = e^{\beta\mu} \sum_{b=1}^{r} \int \delta(\bar{r} - \bar{r}_b) \prod_{i=1}^{r-1} e^{-\beta V_b(|\bar{r}_{i+1}-\bar{r}_i|)} \prod_{i=1}^{r} e^{-\beta V_{ext}(\bar{r}_i)} d\bar{r}_1 d\bar{r}_2 \cdots d\bar{r}_r \tag{2.35}$$

Enforcing a fixed bond length, b, $e^{-\beta V_b(|\bar{r}_{i+1}-\bar{r}_i|)} = \delta(|\bar{r}_{i+1} - \bar{r}_i|) - b)$, we get:

$$n_{eq}(\bar{r}) = e^{\beta\mu} \sum_{b=1}^{r} \int \delta(\bar{r} - \bar{r}_b) \prod_{i=1}^{r-1} \delta(|\bar{r}_{i+1} - \bar{r}_i|) - b) \prod_{i=1}^{r} e^{-\beta V_{ext}(\bar{r}_i)} d\bar{r}_1 d\bar{r}_2 \cdots d\bar{r}_r \tag{2.36}$$

Due to the computational cost of solving this equation, especially the multiple integrals required for calculating the monomer density of long chains, propagator approaches are recommended. [56] It is convenient to use a chain propagator function c(i;r) to handle the bonding potentials. The bonding kernel is first defined as,

$$T(|\bar{r} - \overline{r'}|) = \delta(|\bar{r} - \overline{r'}| - b) \tag{2.37}$$

where we have set a fixed bond length b. For an ideal dimer, we then get:

$$N_{eq}(\overline{r_1}, \overline{r_2}) = e^{\beta\mu} e^{\beta V_{ext}(\overline{r_1})} T(|\overline{r_1} - \overline{r_2}|) e^{\beta V_{ext}(\overline{r_2})} \tag{2.38}$$

and

$$n_1(\bar{r}) = e^{\beta\mu} e^{-\beta V_{ext}(\bar{r})} \int T(|\bar{r} - \overline{r'}|) e^{-\beta V_{ext}(\overline{r'})} d\overline{r'} \tag{2.39}$$

with a total monomer density $n = n_1 + n_2 = 2n_1$. For long chains, the c function approach is defined, which relates to the bonding kernel through the following equation,

$$c(i; \bar{r}) = \int c(i-1, \overline{r'}) T(|\bar{r} - \overline{r'}|) d\overline{r'} \tag{2.40}$$

starting with $c(1,\bar{r}) = e^{-\beta(\frac{V_{ext}(\bar{r})}{2})}$ for the first half-monomer and $c(2,r) = e^{-\beta\frac{V_{ext}(\bar{r})}{2}}$ $\int c(1,\bar{r})e^{-\beta\frac{V_{ext}(\bar{r'})}{2}}T(|\bar{r}-\bar{r'}|)d\bar{r'}$, for the second segment, connected to the first. The rest of the c functions, for different segments are built up similarly. By multiplying the c functions for suitable segments, we can calculate the site densities along the chains.

We note that in a case where grafted polymers exists, additional constraints are considered. We treat this by inserting these constraints as constant potentials, which effectively behave as Lagrange multipliers, adjusted so as to generate the desired grafting density. It is also possible to treat non-ideal (interacting) monomers whereby density distributions have to be established by iterations, until the solution is found.

PB-DFT

DFT can also be used for modelling a dispersion containing ions. In a pure mean field, point-ion limit, the predictions are identical to those from non-linear differential-equation PB theory. The advantage of using DFT is the ease of extension to account for correlations, which are beyond the scope of the mean-field. Having ion species α and λ, we can formulate the pure mean-field functional as,

$$\begin{aligned} F_{PB}[n_\alpha] &= k_BT\int\sum_\alpha n_\alpha(\bar{r})(ln[n_\alpha(\bar{r})]-1)d\bar{r} + \frac{1}{2}\int\int\sum_\alpha\sum_\lambda n_\alpha(\bar{r}) \\ &\quad n_\lambda(\bar{r'})\phi_{\alpha\lambda}(|\bar{r}-\bar{r'}|)d\bar{r}d\bar{r'} + \int\sum_\alpha V^\alpha_{ext}(\bar{r})n_\alpha(\bar{r})d\bar{r} \end{aligned} \tag{2.41}$$

The first term describes the entropic effects, the second term is accounting for the energetic interactions (ES) and the last part adds the effects from external potentials on ions. For one dimensional (planar) geometries, we can integrate out the x and y directions which yields the integral to vary as a function of z direction. Minimizing the grand potential, we arrive at: [56]

$$n_{\alpha,i+1}(z) = e^{\beta\mu_\alpha}.e^{-\beta z_\alpha e\Psi_D}.e^{-\beta V^\alpha_{ex}}.e^{-\beta\sum_\lambda\int_0^D n_\lambda(z')\phi^{(1)}_{\alpha\lambda}(|z-z'|)dz'} \tag{2.42}$$

This equation needs to be solved iteratively. Ψ_D is the Donnan potential, which is iteratively adjusted to ensure electroneutrality.

2.6 Monte Carlo simulations

Evaluating the average parameters, as discussed, is computationally demanding for realistic model systems. The analytical ways to calculate a multidimensional integral are difficult and in such cases, numerical approaches are commonly used. In many cases, even numerically and with assumptions such as pair-wise additivity, the calculation can be costly. If we are interested in finding average quantities, a Metropolis Monte Carlo (MC) algorithm is a viable option. In a simple MC technique, random moves are accepted/rejected via a scheme that generates Boltzmann weighted configurations, over which the average of a desired variable is calculated. Using MC, large free energy barriers can be tackled, which can significantly improve the efficiency of the calculations.

The Metropolis method

In the Metropolis method, sampling is subject to Boltzmann weighting. This means that the probability for a configuration $\bar{r}^N$ in the canonical ensemble is proportional to $exp(-\beta U(\bar{r}^N))$, the Boltzmann factor. It is important to note that using a simple MC code, the configurational integral can not be solved and instead the averages are calculated. By setting the initial configuration ($\overline{r_0}^N$) and its corresponding energy ($U(\overline{r_0}^N)$), the Metropolis algorithm can be summarized as below,
a) a particle is randomly chosen and moved to a new position, with new configuration of ($\bar{r}^N$)
b) the energy of the given configuration, $U(\bar{r}^N)$, is calculated
c) the energy of the old and the new position will be compared by calculating the term, $\Delta U = U(\bar{r}^N) - U(\overline{r_0}^N)$; if $\Delta U < 0$, the move is accepted and the coordinates will be updated; if $\Delta U > 0$, the factor $exp(-\beta(U(\bar{r}^N) - U(\overline{r_0}^N)))$ is compared with a random number, $0 < \xi < 1$. The move is accepted for values larger than the random number; otherwise, it's rejected. The loop is then repeated from (a).
Sampling of, for instance, pressure and energy, is performed randomly now and then, but with a selected frequency.

Periodic boundary conditions

When simulating the system, a selection of N particles in unit cell is chosen as a sample. If this cell is terminated along the edges, there will be large surface effects. To avoid this, particles leaving the box at one side will be replaced by new particles entering the box from the opposite side. Therefore, this can be pictured as replicas surrounding the central (unit) cell, where periodic boundary conditions (PBC) are applied, as illustrated in figure 2.1.

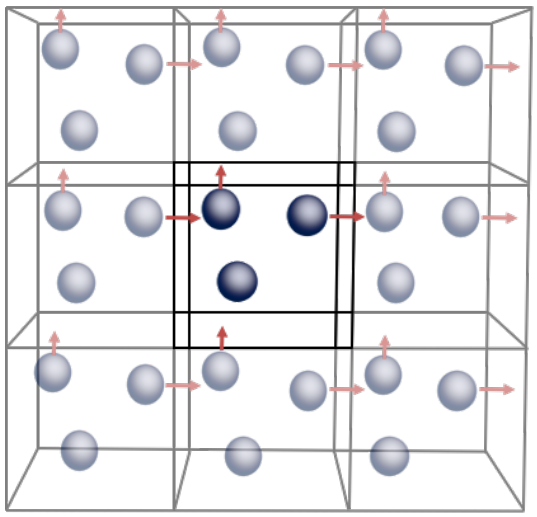

Figure 2.1: The schematic of periodic boundary condition (PBC). Particles exiting at one side must enter from the opposite direction.

Trial moves

In our work on structural properties of colloidal dispersions with isotropic pair interactions composed of a long-ranged repulsion, and a short-ranged attraction, we utilised four different trial moves in order to increase the sampling efficiency. These moves included translational (large and small displacements), completely random move, cluster move, and AVBMC (the aggregation-volume-bias Monte Carlo) move. The last type was only included in a subset of our simulations.

Translational move: a particle with coordinates (x, y, z) are attempted to be moved to a position at $(x + \Delta(\xi - 0.5), y + \Delta(\xi - 0.5), z + \Delta(\xi - 0.5))$, where Δ determines the maximum displacement, and ξ is a random number between 0 and 1. The displacement should not be too small, in order to keep the efficiency at a good rate and not too large, whereby the acceptance ratio becomes small.

Random move: This allows particles to move to a random position within the simulation box. This means that large free energy barriers may be tackled which sometimes improves the sampling efficiency.

Cluster move: a cluster is a collection of particles located in a sphere, of radius R, surrounding a selected (tagged) particle. The entire cluster, i.e. the tagged particle and its neighbours (cluster parameters), is then allowed to move. The size of the cluster may be determined from a previously calculated g(r). R, in our systems, is randomly selected between 0 and R_{max}, where R_{max} is chosen large enough to include all the possible neighbours around the tagged particles. If it is chosen too large, then particles from other clusters will often be

included in the cluster sphere, in which all particles are displaced. Such a move will often change the existing cluster size which will not fulfil the criterion of detailed balance, that is subsequently corrected for, so that the configurations acquire the appropriate Boltzmann weight. Hence, such moves will not be accepted. The cluster move is thus always rejected if new members enter the cluster after the move. [64]

AVBMC move: Similar to the conventional MC, the moves in AVBMC are unphysical and are chosen to improve the sampling efficiency, by inserting a bias factor. The AVBMC is described further in the last work. [65].

2.7 Radial pair distribution function

The structures of materials, whether solid, liquid or gas, are dependent on the intermolecular interactions between the components. In colloidal dispersions, solid or gas-like phases can form as a result of experimental conditions. If we consider a central particle with a shell of particles in its surrounding, with a thickness of dr, at a distance r, the density of particles within this layer can be characterized by a function called as the radial pair distribution function, or g(r). $\rho g(r) dv$ then gives the mean number of particles within this shell volume, dv, with ρ denoting the bulk density. The peaks in the graph represent correlated neighbours, surrounding the particle. The g(r) can be stated in the form $g(r, \rho, T)$, as the density distribution can change with temperature, and bulk density, as well as distance. The radial distribution of particles correlates with the interparticle interactions through the following equation,

$$W(r) = -kTln\left[g(r)\right] \tag{2.43}$$

W(r) is the potential of mean force. The radial distribution function of a system can thus give us structural information about the dominating entropic and energetic forces. For solid materials, peaks are positioned discretely, corresponding to the ordered structures of a solid, whereas for an ideal gas, g(r) = 1. Multiplying g(r) by ρ, we can find the density distribution function, $\rho(r)$.

2.8 Geometry

The geometry we choose to investigate the thermoresponsive properties of particles includes two planar surfaces to which polymer chains are grafted. There are also 'free' chains. The interactions between particles are then calculated using the Derjaguin approximation, which

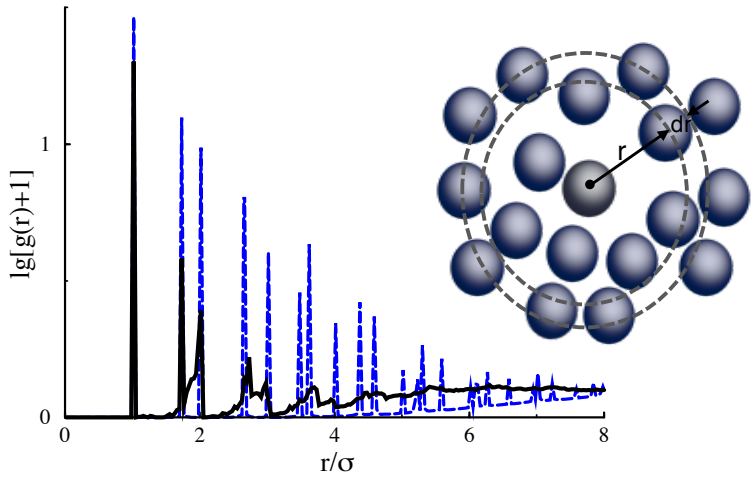

Figure 2.2: The radial distribution function describing the density distribution of particles around the tagged particle.

relate the forces between two curved surfaces, F(D), to the free energy between two flat surfaces, W(D), D being the distance between the planar surfaces,

$$F(D)_{sphere} = 2\pi R_{eff} W(D)_{planes} = 2\pi \frac{R_1 R_2}{R_1 + R_2} W(D)_{planes} \tag{2.44}$$

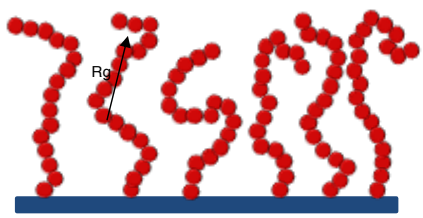

Figure 2.3: The geometry used in the studies describing the planar surfaces to which polymers are grafted.

where R_1 and R_2 is the radius of two spheres with the condition that $R_1 \gg D$ and $R_2 \gg D$. This relation can be used for any types of forces. Smaller particles, as evident, generate a weaker interaction (for instance a weaker barrier height and minimum depth). [59]

2.9 Capillary induced phase transition

The DFT model can be modified to include the effects from capillary interactions in porous media and their effects on phase transitions of simple monomeric solution confined in capillaries. We adopt a DFT which treats the monomers as hydrophobic or hydrophilic using a monomer degeneracy state probability, P, and a degeneracy, g. The geometry is planar surfaces which are immersed into a solution of monomers and solvent particles. The free energy functional F can be found as,

$$\begin{aligned}\beta F &= \int (n_t - n(\bar{r}))ln[1 - n(\bar{r})\sigma^3] + n(\bar{r})ln[n(\bar{r})]d\bar{r} + \beta U[n(r), P_A(\bar{r})] \\ &+ \int n(\bar{r})(1 - P_A(\bar{r}))ln[\frac{1 - P_A(\bar{r})}{g_B}]dr + \int n(\bar{r})P_A(\bar{r})ln[\frac{P_A(\bar{r})}{g_A}] \\ &+ \beta \int n(\bar{r})P_A(\bar{r})\,V^A_{ext}(\bar{r}) + n(\bar{r})(1 - P_A(\bar{r}))\,V^B_{ext}(\bar{r}) + \\ &(n_t - n(\bar{r}))\,V^S_{ext}(r)dr \end{aligned} \tag{2.45}$$

where $n(\bar{r})$ is the monomer density at $\bar{r}$, whereas $n_t - n(\bar{r})$ is the solvent density, and $V^{(\alpha)}_{ext}$ is the external potential exerted from surface on species, where α is either solvent(S), a solvophilic monomer (A) or a solvophobic monomer(B). The assumption is that the overall solution is incompressible, with density n_t. The density distributions can then be obtained from free energy minimization, from which the phase diagram is acquired. Further description of the model is found in the result section.

Chapter 3

Experiments

3.1 Synthesis

In this chapter, we summarize protocols used for synthesizing colloidal particles grafted with a layer of polymer. Synthesis of particles possessing a responsive shell involves methods such as grafting to and grafting from, [28] which is a bottom-up approach to grow shell chains from scratch (from monomers) or synthesizing particles through techniques such as precipitation reaction, dispersion, emulsion, and suspension polymerization. In the latter case, a polymer is fed into the reaction medium to stabilize the propagating particles. The assembly and micellar formation from block copolymers is another way to synthesize grafted particles. We have utilized a dispersion polymerization for synthesizing PEG grafted PS particles aimed at preparing thermoresponsive particles. We were guided by a work performed by Shay et al [23, 24] for the synthesis. We also performed an amine reaction for grafting a functionalized PEG to pre-synthesized PS particles carrying a short carboxylic acid ligand, with the aim to analyse the effect of grafts on particles having a fixed core size.[66] We will explain the protocols in the following sections. Purification of particles as a post-treatment for further analysis will also be discussed.

Dispersion polymerization of PS

Synthesis of particles was performed using a free radical dispersion polymerization of styrene in the presence of PEG as a stabilizer. The PEG terminated with a urethane ligand was initially functionalized [23, 24] and was added to the flask containing water/propanol as a dispersant medium. The solution was then allowed to dissolve completely under a reflux condition. The solution of initiator dissolved in styrene monomer was separately prepared,

and fed into the reactor through a step-wise addition, or all at once, either of which resulted in similar properties. Hence, we continued with the latter approach. Constant stirring was also necessary for preparing monodispersed particles. In order to facilitate fluorescent imaging, we were required to make a small variation to this procedure, by encapsulating a polymerizable dye in the particle cores. To this aim, a methacryloxyethyl thiocarbamoyl rhodamine b dye was separately dissolved in a portion of propanol used for polymerization and was injected after the addition of monomers. Right after the synthesis, samples were passed through glass wool to remove aggregates, or precipitated solid. In order to further get rid of impurities, dialysis against water was performed, using a dialysis membrane. We could use a polymer solution instead of water to induce a larger osmotic pressure and a fast dialysis. However, given that it took almost a week to reach the desired result, we refrained from this procedure and used water, in order to lower the risk of contamination. The particles were then stored for further tests. The particle volume fraction was adjusted using centrifugation.

Amine reaction

In an effort to synthesize PEGylated particles fixed at a core radius, we utilized an amine reaction, explained in a recent work by Stradner et al [66], through which an amine functionalized PEG was covalently grafted to the surface of presynthesized carboxylated PS particles. Carboxylated particles were purchased and used for further experiments. Prior to the synthesis, the particles were dialysed using mini dialysis devices, in order to remove any traces of chemicals used in manufacturing, which might affect particle PEGylation and stability. Glycine solution was prepared separately, by adding a proper amount of sample in water, used to neutralize the catalyst, EDC. Besides, an MES-buffer was prepared at the pH required for the experiments, by adding a proper amount of MES-hydrate in water. The detailed description of materials and procedure used can be found elsewhere. [66] Amine-PEG solutions at different concentrations were also prepared in water. Using a catalyst, EDC, amine-PEG was grafted to the particles. Further dialysis was used for sample purification.

Buffer preparation

The buffer solutions of citrate-phosphate, display buffering capacity within a pH range of 2.6-7, and phosphate, with capacity in the range of 5.8-8 were prepared as follows. The citric acid 0.1 M was prepared by dissolving 1.92 mg in 100 ml miliQ-water. The dibasic sodium phosphate 0.2 M was prepared by dissolving 3.56 mg in 100 ml water. Proper portions of these solutions were then added to adjust the pH at 3 and 4.6. In similar way, stock solutions of 0.1 M = 100 mM of sodium phosphate monobasic and sodium phosphate dibasic was

prepared by adding 1.38 gr and 1.78 gr of each respectively in 100 ml DI miliQ water. These buffers were then used as a solvent for CIPS experiments to disperse PNIPAM/silica samples. Further pH adjustment was carried out by addition of 1 M HCl or NaOH.

Analysis

We here provide some notes on observations we made throughout the experiments, especially the parts lacking the sufficient materials for a thorough study. For visualization and imaging, we used confocal microscopy, which is similar to other optical microscopy in that it captures the images with visible light. The particles used in the experiments had diameters of about 210 nm therefore we were quite aware that individual particles might not be detected by the microscope. However, as we aimed at characterizing the aggregates when formed, yielding the overall aggregate size detectable by the confocal microscope, we could still utilize confocal imaging for the measurements.

In the first study we made efforts to incorporate florescent dye in the particles. We used a dispersion polymerization for the synthesis, hence any choice of dye whether hydrophilic or hydrophobic could not yield a sufficient incorporation, with strong enough florescence response. This was due to the fact that portions of water/alcohol was used as medium and incorporation of dye into either of phases did not result in appropriate outcomes. We therefore mainly used bright field mode for imaging, rather than the florescent imaging.

In the study of CIPS, and to create capillaries, a condensate of silica particles or pellets was prepared by the use of centrifugation. The space between the particles should hopefully display a decent resemblance of capillaries. One form of silica used for this purpose was particles dispersed in suspension which resulted in gel formation upon increasing the concentration or pellet making. This then resulted in pellet networks (gel), which possessed high water contents. Therefore, as the water content changed, adjusting the PNIPAM concentration for the CIPS experiments using NMR was not possible. In other words, the concentration of PNIPAM solution after particle addition (in pellets), extracted from the NMR peaks, varied quite substantially compared to that in the bulk solution. Therefore, we could not produce reliable results using the silica sol for CIPS experiments. We then chose to work with mesoporous silica for analysis.

Silanization of flat surfaces is usually performed through wet and dry deposition. For particles, however, only wet approaches could be used for an even distribution of silane agent. The silane agent with hydrophilic and hydrophobic groups may be utilized for grafting to the particle surface. We prepared different hydrophobized silica using an approach described in a work by Kulkarni et al.[67] Highly hydrophobic surfaces, with low surface affinity toward water, were obtained even with a small silane coating, which could no longer remained dispersed in water. We note that pH could be adjusted to increase the particle

stability. However, as we needed to maintain the pH at low values in order to reach at the hydrophobicity required for the CIPS measurements, we avoided the silanization here and instead adopted pH regulation using buffers at different pH to adjust the surface hydrophobicity.

The rest of the observations are summarized in the research papers.

Chapter 4

Experimental Techniques

In this chapter, a number of experimental techniques for sample characterization will be discussed. Scanning and transmission electron microscopy were used for surface morphology study and measurement of the size and shell thickness. NMR was used to assess the PEG functionalization and also to measure grafting density and further to measure phase transitions in the CIPS study. DLS was used for measuring the size, polydispersity and zeta potential of the particles, and also for studying the temperature-dependent aggregation. We have furthermore used CLSM to directly image particles at elevated temperatures, in order to analyze the structural properties of aggregates.

4.1 DLS

Scattering techniques are classified into two categories, static and dynamic scattering. In static methods, such as SLS, SAXS and SANS, the intensity of the scattered light is measured as a function of the wave vector, q, described below. In dynamic methods, the fluctuating intensity is monitored against time.

The, $\vec{q}$, scattering vector can be calculated by subtracting the scattered vector from the incoming vector. The magnitude of this wave vector can be measured as follows,

$$q = \frac{4\pi n}{\lambda} \sin(\frac{\theta}{2}) \tag{4.1}$$

where θ is the angle at which the incoming radiation scatters, n is the refractive index of the solvent and λ is the wave length of the incoming radiation. It is apparent from the equation that with a fixed solvent and source beam, the magnitude of the wave vector varies as

a function of θ. The source in the scattering methods, can be a beam of light, or x-ray or neutron radiation. Depending on the structural properties and interactions in the solution, the intensity of the scattered radiation fluctuate, and is detected by a downstream detector. The intensity is then related to the q vector, as in static measurements, or is calculated as a function of time. Here, the dynamic light scattering will be discussed in more detail.

In dynamic light scattering, the source of radiation is a beam of photons and the intensity fluctuation of the scattered light is monitored over time. The scattering occurs as a result of the refractive index mismatch between solvent and particle. Due to diffusion processes or intra-molecular mobilities, the local densities/concentration of particles changes and results in a collective fluctuating intensity, which enable us to extract dynamical properties of the solution such as the diffusion coefficient. The intensity correlation function (second order), $G_2(q,\tau)$, is the average integral over the product of intensities at time t and t+τ,

$$G_2(q,\tau) =< I(t)I(t+\tau) > \tag{4.2}$$

where I(t) and I(t+τ) are the intensity at time t and t+τ, respectively, and τ is the lag between these times.
The intensity correlation function can then be normalised as follows,

$$g_2(q,\tau) = \frac{< I(t)I(t+\tau) >}{< I(t)^2 >} \tag{4.3}$$

The field correlation function, $g_1(q,t)$ (first order) can be related to the autocorrelation function of the electric field through Siegert relation,

$$g_1(q,\tau) = \sqrt{\frac{g_2(q,\tau)-1}{\beta}} \tag{4.4}$$

where β is the coherence factor which is dependent on the detector. In fact, in light scattering methods, where the measurement of the motions is not precisely known, we can instead measure the electric field variations by means of fluctuations of the scattered electric field. The autocorrelation function describes the motions of particles or molecules. For a monodisperse system, the diffusion coefficient can be extracted from the following equation,

$$g_1(q,\tau) = e^{-Dq^2\tau} \tag{4.5}$$

where D is the collective diffusion coefficient. The term $-Dq^2$ is the decay constant.
At dilute conditions, D measures the self-diffusion coefficient and the hydrodynamic radius, R_h can be calculated using the Stokes–Einstein equation,

$$D = \frac{k_B T}{6\pi\mu R_h} \tag{4.6}$$

where k_B is the Boltzmann constant, T is temperature, and μ denotes the viscosity of the solvent.
For a polydisperse system, we have used the cumulant analysis method [5], which provides a mean value for the diffusion coefficient.

$$\ln g_1(q,\tau) = -(-Dq^2)\tau + \frac{k_2}{2!}\tau^2 - \frac{k_3}{3!}\tau^3 + \frac{k_4}{4!}\tau^4 ... \tag{4.7}$$

where k_2, k_3, and k_4 are the second, third and forth coefficients of a forth order cumulative expansion. Usually, with a good approximation, the R_h and PDI can be calculated by the second cumulant expansion.
The DLS measurements in this work was performed using a Malvern Zetasizer, equipped with a He-Ne laser with λ= 633 nm and a detector positioned at scattering angle of 173°.[5]

4.2 CLSM

Confocal laser scanning microscopy has been widely applied for studying biological samples, and, with some restrictions, for phase behaviour analysis of colloidal dispersions. This is due to the fact that the wave length of the laser for sample illumination is in the range of visible light and imaging of particles with small sizes might be limited. Despite the limitation, this method is utilized here to monitor cluster formation and structural behaviour of dispersions rather than tracking an individual particle. Besides, one advantage of confocal microscopy over the scattering techniques is that it allows us to directly look into the samples, which facilitates analysis of movements and aggregation at equilibrium conditions as well as dynamical studies of colloidal particles.

Similar to a conventional microscope (an advanced version), in confocal microscopy, a laser is used to illuminate the specimen. Light is directed by mirrors toward the sample. Due to the interaction between light and the sample, the incoming light becomes reflected and is then recorded by a downstream detector, to construct the image. In a confocal microscope, however, a pinhole is placed between the detector and the sample, in order to remove the

out of focus lights which contribute to a low quality/blurry image. By filtering out the undesired emissions/lights, the sharply focussed slices form a high resolution image. The source of radiation in the conventional microscope is often UV light whereas in confocal microscopes, the lasers emit visible light. Another feature of confocal microscopy is that for liquid samples showing dynamical changes, time series can be constructed with resolution in the range of microseconds.

An appropriate sample thickness is required for imaging, approximately 10 μm, which is to reduce possible light interferences and to produce high quality snapshots. The imaging then is carried out by scanning through the x-y plane and in the z-direction. The quality of the images depends on the optics, the pinhole and the pixel size. One quality-related feature is the resolution which is defined as the smallest distance that can be resolved by the microscope. The resolution limit in conventional and confocal microscope differs and is summarized in table 4.1.[68] In order to compare a conventional and a confocal microscope, the resolution for both cases are defined, in z-direction and on x-y plane.

Table 4.1: The comparison of resolution between conventional and confocal microscopy

-	Conventional microscope	Confocal (PH>1 U)	Confocal (PH <0.25 U)
z-direction	$(\frac{1.67n\lambda_{em}}{N^2})$	$(\frac{0.88\lambda_{exc}}{n-\sqrt{n^2-N^2}})$	$(\frac{0.64\overline{\lambda}}{n-\sqrt{n^2-N^2}})$
z-direction (N<0.5)	$(\frac{1.67n\lambda_{exc}}{N^2})$	$(\frac{1.67n\lambda_{exc}}{N^2})$	$(\frac{1.28n\overline{\lambda}}{N^2})$
x-y plane	$(\frac{0.51\lambda_{em}}{N})$	$(\frac{0.51\lambda_{exc}}{N})$	$(\frac{0.37n\overline{\lambda}}{N})$

The PH is pinhole diameter in unit of U (Airy unit), N is the numerical aperture of the objective, λ_{em} and λ_{exc} are the excitation and emission wavelength, and n is the refractive index of the medium. According to the expressions, the resolution is higher for the confocal microscope, when the pinhole is used.

The imaging parameters used here are the numerical aperture of N=1.4, λ_{exc}=543 nm, λ_{em}=660 nm. Specifying these quantities, the resolution in x-y plane and z-direction becomes 171 nm and (428, n=1) 556 (n=1.3) nm, respectively.

4.3 Electron microscopy

Electron microscopy is a powerful technique for structural studies of solid materials, which are being characterized by atomic distances of 0.2-0.3 nano meter. The resolution limit of an optical microscope, which is approximately 200 nm, prevents structural studies of solid

materials at an atomistic level. Even compound microscopes with multiple lenses or the use of oil immersion objectives for decreasing the wave length of the ray (by a factor of 1/n (refractive index)), cannot be applied for studying atomic distances.
The limitation can be described in terms of magnification which is defined as resolution per the actual size of the object. To resolve an object with size of a few nano meters (for example in case of biological samples) using an optical microscope, the magnification must be larger that 1500 x, the original size, which is the limit of an optical microscope. The advent of electron microscopes has enabled us to overcome this limitation. The wavelike feature of electrons can, according to Louis de Broglie, be related to the electron momentum, $\lambda = h/mv$, where h=6.626 10^{-34} (m^2kg/s) is the Planck constant and mv is the momentum of an electron (mass and velocity). The energy of an electron can be increased by an accelerating potential, thereby reducing the wave length, causing electrons to penetrate distances in the range of atoms into solids, whereby an improved resolution is obtained. The diffracted rays from the atoms can then be detected and resolved to form an image. In addition, due to the negative nature of the charges, which are deflected by electric and magnetic fields, electrostatic lenses carrying an electric current can be used to image the electrons.
The specimen in a electron microscope is in a dry state and is imaged by radiating electron beams onto the samples. Transmission electron microscopy (TEM) and scanning electron microscopy (SEM) are the two main classes of electron microscopy.
In TEM, which was developed earlier, the beam of electrons passes through a thin specimen ($< 200nm$). It interacts with atoms, and, after being deflected, all the electrons (deflected or non-deflected) are imaged. The primary electrons might provide energy to the electrons of the specimen, and cause them to radiate, known as secondary electrons. This then causes a fraction of the primary beam to penetrate the samples and a fraction to be backscattered. The transmitted electrons, backscattered, and secondary electrons are then collected by appropriate detectors, to provide information for characterizing the sample. The resolution of a TEM microscope is 0.2 nm, with the accelerating voltage between 100 kV and 300 kV. Imaging samples with large thickness is a limitation of a TEM microscope. Due to the fact that the secondary electrons cause difficulty in focusing the electrons by the lenses, image quality can be affected. An alternative way of handling the secondary electrons for creating an image is scanning the specimen which is the basis of SEM, i.e. scanning the area in two perpendicular directions and collecting the secondary electrons to create the image. These electrostatic and magnetic lenses are used for focusing the electrons. The image resolution of SEM is between 1 nm and 10 nm. [69]

4.4 NMR

The atomic nuclei possess a property known as 'spins'. These effectively act as small bar magnets which can align in an applied magnetic field, from which information on properties of matter can be extracted. In contrast to other spectroscopic techniques where an intensity ray can generate transitions between existing energy levels, in nuclear magnetic resonance spectroscopy (NMR), the energy levels of spins in atoms (excitation in atoms) are created using applied magnetic fields. These levels depend on the chemical environment, leading to chemical 'shift'. The intensity and chemical shifts of the spins in atoms such as 13C, 1H, and 15N give us valuable information about the structural and dynamic properties of samples and also identifying molecules and reactions in solid and liquid samples. The most common NMR experiments include 13C and 1H NMR, as the nuclei of these atoms possess spins with a quantum number of I=1/2, whose local magnetic field change by applying a magnetic field. The development to the regular 1-D NMR spectroscopy, is the 2-D NMR which is applied for identifying neighbouring groups, based on the coupled spins. The resonance frequency, ν, can be measured according to the following equation,

$$\nu = \frac{\gamma B_0}{2\pi} \tag{4.8}$$

where γ is the gyromagnetic ratio of the nucleus, and B_0 is the strength of the magnetic field along the z axis. The energy difference, ΔE, is then product of ν and Planck's constant, h. If this energy is equivalent to the energy difference between nuclear states for instance α and β, the energy required for flipping the spins is,

$$\Delta E = h\nu \tag{4.9}$$

ΔE, or ν, can be detected in an NMR experiment.
For detecting the signals in an NMR experiment, a radio frequency (RF) signal with an oscillating field with magnitude of B_1 is applied along x or y directions for a certain time to excite the nuclei; spins are then left to decay over time (due to the relaxation) to equilibrate. The intensity of the decaying pulse (in time domain (free induction decay, FID)) is recorded and is then Fourier transformed to frequency domain signals (spectrum), to provide the chemical shifts. In a typical NMR experiment, the RF is usually chosen as a 90 $^\circ$ pulse perpendicular to the applied magnetic field, B_0. The magnetization can then be tipped out to the x-y direction, in order to be measured by the phase difference, θ. The length of the pulse, t_p, can be related to θ. The case where $\theta =$ a 90 $^\circ$ is known as a 90 $^\circ$ pulse.

$$\theta = \gamma B_1 t_p \tag{4.10}$$

The relaxation of spins can provide important information about the physical and dynamic properties of molecules.

Chapter 5

Results

In this chapter, we summarize the main findings of the work performed throughout this thesis including the results from the publications. The thermoresponsive behaviour of dispersions containing particles and polymers were investigated through combinations of experiments and theories.

5.1 Building polymer-like clusters from colloidal particles

Recent works on assembly of particles have addressed the anisotropy in structure resulting from the interaction potentials, which are radially symmetric. In particular, a short-ranged attractive potential combined with a long-ranged repulsive barrier is shown to generate polymer-like clusters in a way that the free energy minimization is achieved by chainwise addition of particles to their neighbours, mainly due to the repelling forces from distant particles. To test this, we have set up experiments and built theoretical modellings of PS particles carrying a thin layer of PEG which, owning to their morphology, are believed to be good candidates for producing the suggested structures. We constructed a coarse-grained model (of experimental dispersions), which utilizes temperature, grafting density, particle charge, and ionic strength as input parameters. The particle-particle Potential of Mean Force (PMF) was then established by classical Density Functional Theory (DFT) calculations, in combination with the Derjaguin Approximation (DA). This model has been validated against experimental data by Shay *et al.* in a previous work[23, 24]. Using polymer DFT and Poisson Boltzmann (PB) DFT, our model of PMF was established. This PMF was then simplified and imported to a Metropolis Monte-Carlo (MC) code, from which we could predict structural properties of dispersions[1]. The reason for building a simple

[1]A 4-parameter model was also established by a fit to the DFT-PMF to simplify the system description.

model was to reduce the complexity, and to facilitate simple interpretations of the results. We then qualitatively compared the results to experimental findings.
The investigation mainly revolved around the thermoresponsive properties of polymer grafts which generate hydrophobic interactions upon heating. Temperature and graft properties, molecular weight (MW) and grafting density were adjusted to control the range and strength of the attractive minimum whereas the shape of the repulsive tail was regulated by the particle charges, and the ionic strength. The range of the repulsive interactions in the model was adjusted by the Debye length, producing a long-ranged repulsion, while the range of the attractive forces, τ, was allowed to vary, as a response to a temperature change. The resulting structures at high temperatures, after an energy plateau was achieved, were clusters composed of PS particles, which aligned almost linearly, although with some degree of branching. The results are illustrated in figure 5.1.

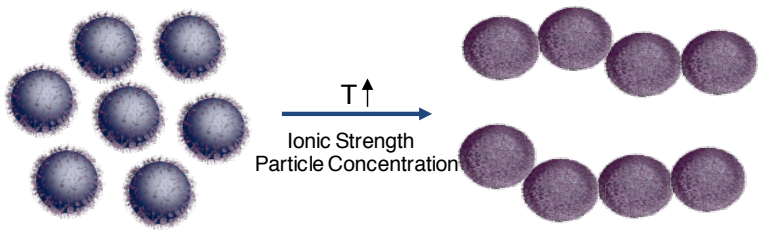

Figure 5.1: Schematic graph depicting the phase transition behaviour of PS particles carrying short grafts of PEG which partly aggregate upon heating, forming polymer-like clusters.

Even though the particles interacted via radially symmetric PMFs, anisotropic clusters were the dominating final structures. Wider minimum values created more compact clusters, with a thicker backbone. By analysing the data, we could predict that a dispersion at low ionic strength, containing weakly charged particles, which are grafted by short chains of a thermoresponsive polymer at small grafting ratios, is a good candidate to produce the suggested results. To test this, we set up an experimental protocol for synthesizing and analysing the particles, where the structural and physical properties of aggregates could be investigated.

The particle size and morphology were optimized using the amount of monomer added to the dispersion. The measured average diameter of the particles was 189 nm and the particle weight fraction was adjusted at 0.04-0.08 wt% for the measurements. Samples of particles showed a satisfactory monodispersity, as the PDI was measured at 0.07, suggesting no significant discrepancy to the assumptions of identical particles, that we made in the simulations. By adjusting the synthesis parameters, we could therefore prepare a suitable dispersion for further analyses.
The samples were then prepared and heated to equilibrate. The temperature response and

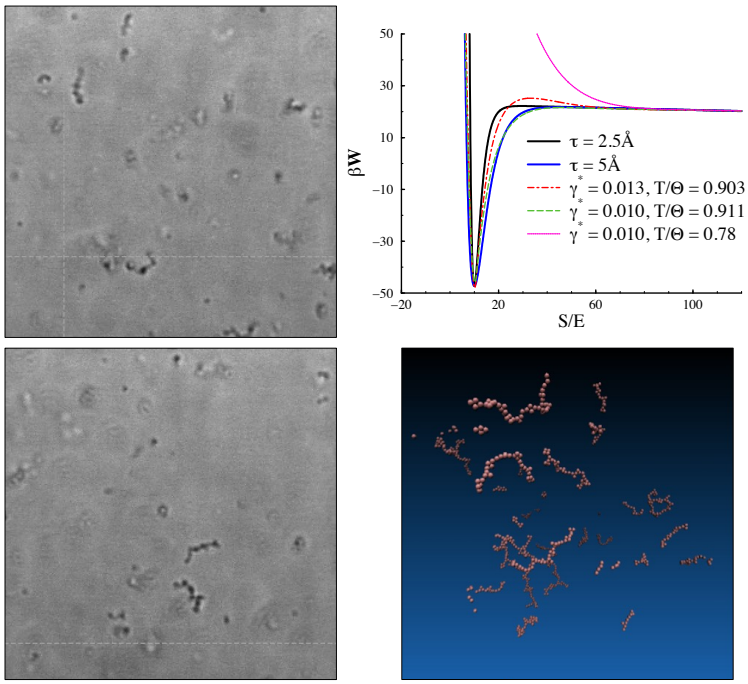

Figure 5.2: The combination results of experiments and simulations showing the phase transition and aggregation of PS particles grafted with PEG. The snapshots on the left side are the confocal images and on the right is the results from DFT and MC simulations, showing the corresponding DFT modelled PMF producing the suggested clusters. θ denotes the theta temperature, which is around 100 °C, for PEG in water τ measures the range of the attractive interactions.

transition of particles were monitored by imaging of the dispersions sequentially, using a confocal microscope. The snapshots of clusters, formed at 'equilibrium' (at least metastable) are collected in figure 5.2. Due to the hydrophobicity change of the monomers, which suppressed the steric effect of grafts, clusters varying in shape and stability were formed across a range of temperatures, and particle volume fractions. In the dilute regimes, roughly linear clusters were found. These structures survived during rather extended equilibration periods (weeks), and were thus at least metastable. The coarse-grained model is also shown in figure 5.2, comprising a PMF that displays a monotonic repulsion at room temperature, which upon a temperature increase changes to include an attractive minimum, which in turn results in particle aggregation. The main outcome here was particles coexisting with linear/polymer-like clusters, with some branching, at high temperatures and low concentrations, where they remained at least metastable as a result of the balanced forces.
In addition to temperature control, we also performed experiments on particles which were exposed to an ion exchange resin (basic type), with an aim to investigate the role of the repulsive barrier on the stability. Particles were then incubated at similar conditions as those

which were previously tested. The results indicated one unit increase in pH which seemed to effectively inhibit the cluster formation. This, in fact, revealed that at low enough ionic strength, the role of the electrostatic repulsive barrier in controlling the stability of particles could be quite significant. Therefore, an alternative to tuning the attractive minimum, was to adjust the range and strength of repulsion, where we could regain particle stability at higher temperatures by adjusting the barrier parameters. Electrostatic screening effect was lost due to the reduced amount of salt, which resulted in an increased Debye length and thereby an increased stability. We note that the main purposes here were to investigate the effect of temperature on the inter-particle interactions. The regulatory effect of PEG as a thermoresponsive polymer on the attractive potential was studied which resulted in strong structural responses, to the cluster formation.

5.2 The non-monotonic temperature dependent behaviour

Particles grafted with a thermoresponsive polymer may display a temperature-dependent aggregation. In this case, the interparticle interactions are tuned by exploiting the thermal properties of polymer grafts and/or added dissolved polymers. At low temperatures, where the dissolved polymers do not adsorb to the particles, the resulting force, known as depletion attraction, arises from osmotic pressure differences between the bulk and the interparticle region. This causes the particles to attract each other. The theoretical modelling of a similar system has been carried out previously, in a work by Fei et al[36], where a non-monotonic temperature response of particle aggregation was observed upon heating. We shall modify that model here to investigate the effect of grafts and also the dissolved polymer on particle interactions. The non-monotonic behaviour was attributed to a change in the thermoresponsive properties of PEG, and its surface affinity, as temperature was increased. At low temperature, addition of a non-adsorbing PEG at a sufficient concentration resulted in particle flocculation, which was driven by depletion interactions, due to the restricted conformational space in the interparticle regions. Temperature increase to values close to the LCST resulted in a more severe aggregation, which was attributed to the attractions arising from adsorbed bridging chains, driven by hydrophobic interactions (via an increased population of hydrophobic monomers, which attract to the particle surfaces). Interestingly, at intermediate regimes, particle redispersion was observed, resulting in dispersions which remained stable. The schematic of this behaviour is depicted in figure 5.3. To test this response, along with the model modification, we carried out experiments on PEG-grafted PS particles, in the presence of dissolved PEG. We monitored the structural responses of particles at different conditions of temperature and concentration, using confocal microscopy. The amount of added PEG to the dispersion was (at low and high temperatures) sufficient to induce aggregation, after equilibrating for one week. The thermal analysis was performed at 45 °C and 75 °C. The results are collected in figure 5.4.

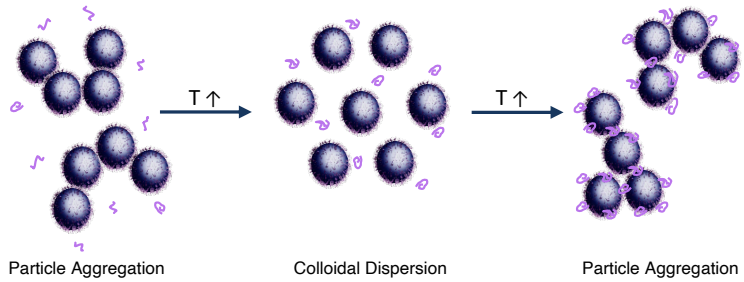

Figure 5.3: Schematic graph depicting the phase behaviour of particle/polymer dispersions upon temperature increase. The particles are grafted and dispersed in a solvent containing dissolved polymer chains. The particles either aggregate or remain dispersed, depending on the temperature.

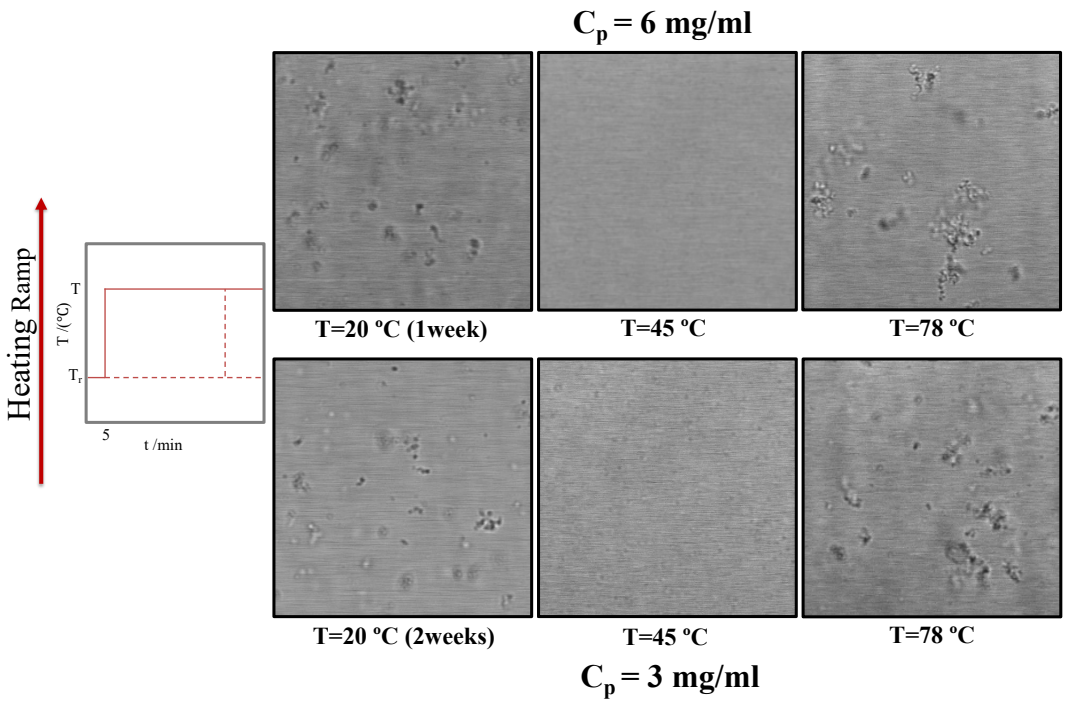

Figure 5.4: The thermal analysis of particles using confocal microscopy in the presence of added PEG at different concentrations, C_p. The left panel represents the thermal analysis using a heating ramp starting at T_r, the reference temperature to T, higher temperatures. The heating profile in dashed line is when particles are allowed to rest at T_r and then are heated to elevated temperatures.

The non-monotonic aggregation response was indeed observed in the experiments, where

we noted a re-entrant flocculation behaviour. In order to establish whether the aggregation was a result of depletion, or bridging interactions, the surface affinity of PEG toward PS carrying short PEG graft was considered. We note that due to the fact that the surface was sparsely grafted, and that the aggregation was non-monotonic, the PS particle surface was hydrophobic. This was supported by flocculation of only grafted particles, at high temperatures, due to the bridging interactions. If grafted PEG in particle dispersions had adsorbed at low temperature due to the bridging, one would expect an increased adsorption (stronger bridging) as temperature gradually is increased. However, this was not observed and the grafted particles at low temperatures remained stable. This was associated to the presence of hydrophilic monomers not being adsorbed at hydrophobic surface which then contributed to steric stabilization of the particles. Therefore, as the surfaces was hydrophobic, addition of the PEG as a hydrophilic polymer at low temperatures, resulted in particle aggregation due to depletion interactions. This was prerequisite for observing such non-monotonic response, which could only be observed for solvophobic particles (at least with added PEG, in water). Note that PEG becomes increasingly hydrophobic, as the temperature increases. At low temperatures, PEG, composed of hydrophilic monomers was considered non-adsorbing and at high temperatures, populated by hydrophobic monomers, it was considered as adsorbing. We could, however, find an intermediate regime where PEG in contact with surface neither adsorb nor desorb, causing polymer-mediated interactions which were repulsive. Therefore, a non-monotonic trend from non-adsorbing to adsorbing was seen for PEG grafted PS particles and added PEG.

The theoretical calculations were also performed by modifying the pre-established model of DFT on degenerate states of monomers. The more simplified model was utilized here, using a temperature-dependent LJ potential with the aim to reduce the degree of complexity. The chains dissolved and grafted were modelled using polymer DFT. Guided by previously established models, the LJ parameters were adjusted at varying temperatures. We note that this simplification results in a more phenomenological model, unable to capture the mechanistic origin of the increased hydrophobicity, at elevated temperatures. In other words, the level of coarse-graining is taken one step further. In contrast to the results at low and high temperatures, the resulting PMF at intermediate regimes was then purely repulsive which was mainly corresponded to the change in the surface interactions, becoming progressively stronger, going from depletion to bridging attraction.

Discussing this further, we can instead change the adsorption strength at a constant temperature. In order to simplify thing even further, we then consider ideal monodisperse chains connected by bonds of a fixed length b, but where the monomers otherwise are non-interacting ('point-like'). This is a commonly adopted model for polymer solutions at 'theta' conditions. The advantage with this model, apart from being very simple, is that the DFT treatment is exact, i.e. we can obtain exact result, for the given model. We will still utilize two hard and infinite planar confining walls, located at $z = 0$ and $z = h$, and the

fluid is in equilibrium with a bulk solution, as ensured by our grand canonical formulation. We will here also include short-ranged soft interaction, $W(z,h)$, acting on all monomers, with $W(z,h) = w(z) + w(h-z)$, and $\beta w(z) = e(1-z/z_c)^2$, $z < z_c$. Given a fixed value of z_c, which we have chosen as $z_c = b$, we are thus left with a single adsorption parameter, e, describing the surface affinity. The temperature is kept constant, and we set the degree of polymerization to 100. In figure 5.5, we illustrate how the net free energy interaction per unit area, Δg_s, swaps from attractive, to repulsive, as the surface parameter, e, is gradually increased. One might be inclined to think that these results imply that the repulsion is a rather esoteric phenomenon, limited to a very narrow range of conditions, since the relative difference of e is rather small when transition occurs. But one should keep in mind that for a system where the attraction increases with temperature, there will inevitably be an interval with a net repulsion. Furthermore, a temperature range of (say) 350 K to 460 K would not be considered as narrow. We emphasize the generality of these results, i.e. a swap from adsorbing to non-adsorbing conditions (or vice versa) is predicted to *always* lead to an intermediate regime, in which the polymers mediate a repulsion. One experimentally viable option to a temperature change might be a gradual addition of a different solvent.

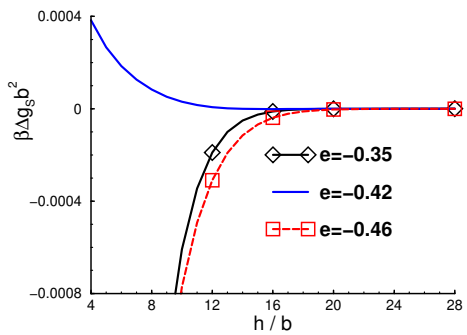

Figure 5.5: The net surface interaction free energies, $\Delta\beta g_s b^2$ for ideal polymers, at various e, surface affinities. The polymers are ideal and monodisperse, with each chain being composed of 100 connected monomers. The results are exact, for the given model.

5.3 Polymer-like self-assembled structures

Previously, we established a DFT-modelled PMF composed of a long-ranged repulsive barrier combined with a short-ranged attractive minimum, suggesting anisotropic (polymer-like) clusters formed by polymer grafted particles. To elaborate on these results, we utilized an Aggregation Volume Bias Monte Carlo (AVBMC)[70] technique with an aim to increase

the sampling efficiency. We performed our simulations on a similar system as described in the first work, but allowing AVBMC to be either utilized or switched off. We started either from a (partly) pre-equilibrated system, or from random configurations, and introduced AVBMC moves to assess particle aggregation. An advantage was that the formed clusters could dissociate, and associate, as a result of an efficient barrier crossing, which was almost impossible to achieve using other types of moves. In other words, clusters were allowed to equilibrate faster. We could therefore approach more stable states by a controlled biasing scheme (including corrections, so as to arrive at the proper Boltzmann weight), so that particles were allowed to move between a selected region ("in" or "bonded" region) to an outside region, with larger volume ("out" or "non-bonded" region). This allowed us to tackle the large free energy barrier which could not be possible using a conventional MC.[70] In a typical MC algorithm, the moves are accepted based on weighing by Boltzmann factor, leading to the following acceptance probability:

$$acc(A \rightarrow B) = min[1, exp(-\Delta U/k_B T)] \tag{5.1}$$

In the AVBMC technique, the moves are preferentially selected, whereby particles are transferred into, or out of, "bonded" region. The "bonded region" is a predefined volume surrounding each particle, within which there is a significant interparticle attraction. As mentioned, such AVBMC moves are preferentially selected, and the acceptance rule for (say) "out" to "in" move must be modified to "counteract" this bias, whereby we end up with properly Boltzmann-weighted configurations:

$$acc(A_{out} \rightarrow B_{in}) = min[1, \frac{(1 - P_{bias}) V_{in} exp(-\Delta U/k_B T)}{P_{bias} V_{out}}] \tag{5.2}$$

with a reversed notation for calculating the acceptance rule for "in" to "out" regions.[70] Here, P_{bias} denotes the probability to attempt a move of a (randomly selected) particle i into the bonded region ("in") of another (randomly selected) particles j, whereas $(1 - P_{bias})$ is the probability for an attempted move of i to the "out" region of j. In our simulations, $P_{bias} = 0.5$, so $\frac{1-P_{bias}}{P_{bias}} = 1$. For in-in (an attempted 'in' move, where i already is bonded to j) and out-out moves, the normal MC acceptance rule, eq. (5.1) is used.
Results of our simulations showed that AVBMC moves had a remarkable impact on structural properties. The final clusters in the presence of AVBMC were seen to be more compact, with less tendency to branch along the backbones. Furthermore, an observed drop of the interaction energy, associated with the introduction of AVBMC moves, suggested that the system then was approaching complete equilibrium. The energy convergence in the absence of AVBMC also appeared to reach a pleateu, or an initial plateu, which made us conclude that the initially formed clusters should be considered as metastable. We hypothesized that the metastable clusters are most likely the resulting structures found in a real experiment.

In figure 5.6, we provide radial distribution functions from simulations, as well as configurational snapshots. The snapshot shows the largest cluster formed for a given collection of simulated particle coordinates, for the case with an attractive range of $\tau = 5$ Å. For a fixed τ, set to 5 Å, we could detect more branched, and larger, clusters in the absence of AVBMC. The RDF graphs for two choices of τ, also showed another interesting result. In the absence of AVBMC, smaller τ values, i.e. narrow attractions, created more short-ranged clusters compared to the larger τ values, as is observable by the tail of the curves. By including AVBMC moves, this relation was reversed, whereby larger τ values ($\tau = 20$ Å), i.e. broad attractions, resulted in smaller and more compact clusters. Therefore, larger τ values resulted in minimal energies with more compact clusters associated which resembled 'Bernal spiral' structures, though these might be unlikely to reach in an experiment.[1]

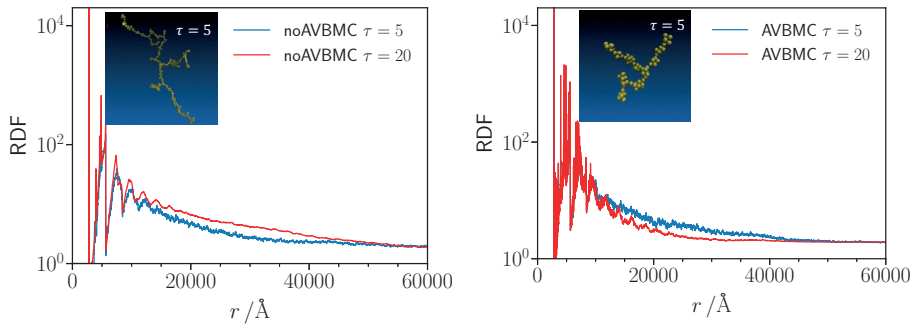

Figure 5.6: The radial distribution function of particles with and without AVBMC move. The simulations was performed at two different τ values, the range of attractive well. The configurational snapshots of clusters from the simulations are also included.

Let us finally investigate the simulation results for a smaller system of particles interacting with a weaker PMF. The PMF, the resulting clusters and the energy convergence with and without implementing the AVBMC move have been collected in figure 5.7. The simulations were in this case faster than those in the published work. The clusters in the absence of the AVBMC possessed narrow backbones with some degree of branching. From the energy convergence, it is obvious that the equilibrium was achieved faster when the AVBMC was applied whereas in the absence of this move, the system could reach a metastable state.

5.4 Confinement-induced phase transitions

In this work, the effect of capillaries on the phase transition of a fluid showing an LCST was investigated. The fluid was a simple monomeric liquid possessing a mixed population of hydrophobic and hydrophilic monomers, whose ratio could be regulated upon temper-

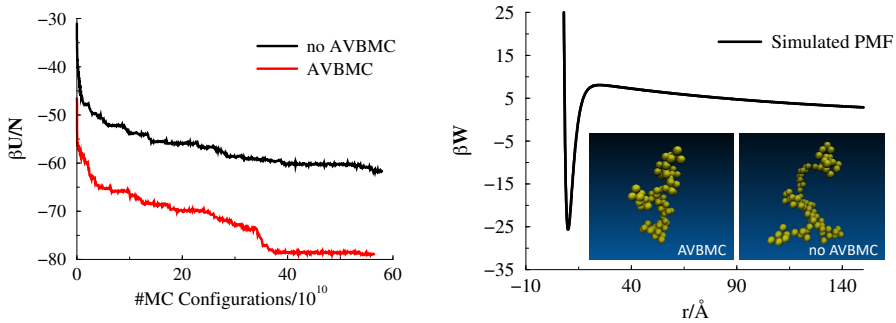

Figure 5.7: The simulation results for a system of 80 particles with a PMF displaying a weaker barrier as well as a less adhesive minimum. The PMF and the energy convergence as well as the snapshots extracted from the vmd software are shown here.

ature variation, becoming more hydrophobic at higher temperatures. The restriction to a mixture of unconnected particles (solvent and monomers) allowed us to produce illustrative simplified descriptions, but the main qualitative conclusions are valid also for polymer solutions, that display an LCST. We used a DFT model to assess the effect of capillaries on phase equilibria and density distributions. The particles interacted via a Lennard-Jones potential. We established capillary induced phase transitions (CIPS), which resulted in coexistence of phases rich and poor in the population of hydrophilic monomers. Due to the surfaces truncating the intermolecular interactions, a shift of LCST to lower temperatures, compared to the bulk, was identified. The transition was not associated to any temperature dependent interactions but rather to the truncations of interactions in the presence of surfaces, which caused the system to behave as if temperature was higher. The transition was characterized by the free energy curves of the phases dilute and concentrated in the number of hydrophilic monomers, showing an intersection when mapping the capillaries of varying widths. The width of the capillary was found to be an important parameter for the resultant phase transition behaviour, showing a more pronounced decrease in the capillary LCST for small gap sizes. We demonstrate the general behaviour of such polymer solutions in the presence of capillaries in figure 5.8 which represents a decrease in the LCST as compared to its value in the bulk.

5.5 Experimental study of carboxylated particles, temperature effect

In addition to the PEG grafted PS particles that we synthesized for the thermal measurements, we also performed experiments on carboxylated PS particles that we received from

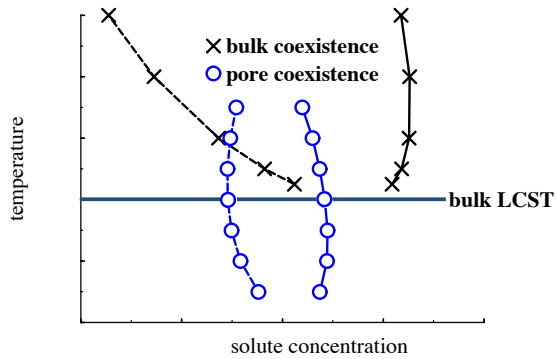

Figure 5.8: The phase diagrams of polymer solutions showing LCST within bulk and pores. The value of LCST is indicated by the blue solid line.

the suppliers. We used an amine reaction to graft a PEG layer to the particle surfaces, using PEG with molecular weights of 2 and 10 kDa. The aim was to regulate the thickness of the grafted layer, and assess its effect on the thermoresponsive properties of particles, having a fixed core size. These particles were then washed and purified for further analyses. Similarly, in order to perform the thermal analysis tests, particles were heated and characterized by DLS and CIPS. Size, thickness of the grafted layer, and the zeta-potential were measured at room temperature, and the results are summarized in figure 5.9. Bare PS particles had the size of 200 nm whereas the size of the grafted particles was ranged from 235-245 nm. This was achieved by adding 50, or 100 mg, PEG to a fixed dispersion volume at controlled experimental conditions, such as the shaking rate, and the amount of catalyst used for performing the synthesis. The particles with a larger size were obtained with an increased amount of PEG. The effect of molecular weight (MW) on the size was not fully assessed. However, a higher MW PEG generated even larger particles, due to the larger graft length. The zeta potential of non-grafted PS was measured as -60 mV, showing that a large number of surface charges provided stabilization, due to the electrostatic repulsive forces. The PEGylation generated near-neutral particles (a weak positive effective charge), which results in a changed stabilization mechanism from electrostatic to steric repulsion. Upon amine reaction, the negative charge of carboxylic groups turned to positive charges corresponded to the amine bonds attached to the surface. Grafted layers of carboxylic acid groups were then replaced by amine-grafted PEG. The particles were purified using extensive series of dialysis in order to remove any chains remaining un-grafted. The zeta potential of particles were then measured, showing reduced magnitudes of the zeta potential after grafting which was associated to the chains being extended away from the surface, i.e. the grafted layer shifts the slip plane further out which results in a decreased zeta potential. We also note that the reduced zeta potential might also be associated to the effect of PEG attaching to the surface

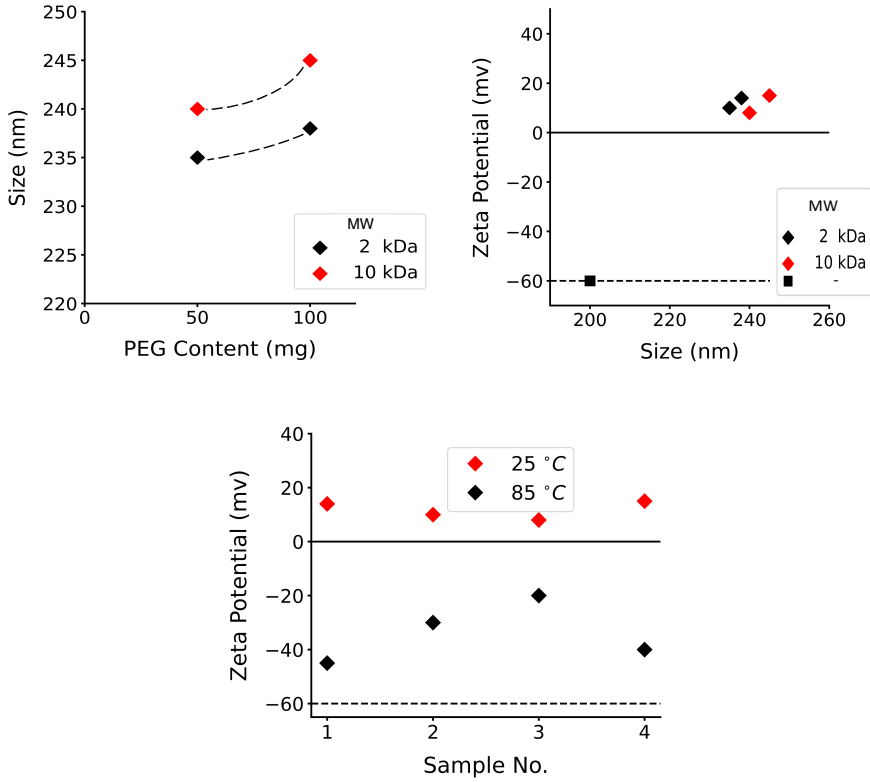

Figure 5.9: The test results of particles grafted with amide-functionalized PEG. The molecular weight of grafts were either 2 or 10 kDa. The results of zeta potential were also compared to the results obtained for bare carboxylated particles with no grafts, indicated with square. The samples 1 and 2 in the bottom panel corresponds to the PEG with MW of 2 kDa and samples 3 and 4 corresponds to PEG with MW of 10 kDa. The dashed lines are for comparison with the reference sample.

physically, where the surface charges are then blocked by grafts. Any physically adsorbed non-grafted chains, however, are amine-functionalized and carry no charges (neutral). The temperature increase caused the thickness of the grafted layer to decrease which resulted in a shift of the Stern layer toward the surface causing a higher values for the zeta potential. Besides, further detachment of polymer chains from the surface (if present), could shift the slip plane closer to the particle surface, resulting in an increased magnitude of the zeta-potential. This was in agreement with the reduced size of particles at elevated temperatures. The effect of MW on the zeta potential was not significant. Since we aimed at reaching qualitative tests on thermoresponsive properties, we did not measure the polymer grafting density or the layer thickness. Therefore, measurements on particle response at elevated temperature were performed using the zeta-potential (DLS) and CIPS. The samples were

stored at low and high temperature, and were imaged using the microscope. There were no sign of aggregation at temperatures up to 85 °C. Even though the particles were grafted with a PEG layer, there were no indication of temperature-dependent response. To further scrutinize this finding, zeta potential measurements were performed at low and high temperatures, on grafted and non-grafted particles. Particles grafted with PEG carried a weak positive charge at room temperature. However, at elevated temperatures, the zeta-potential became significantly stronger, with a negative sign. The increased strength can be related to a reduced thickness of the grafted layer, as the temperature increases. We claim that at low temperatures, a combination of almost neutral particles, but hydrophilic chains, resulted in steric stabilization (weak), whereas at high temperatures, where more compact layers, and strong zeta-potential values were obtained, electrostatic repulsions contributed to particle stability. Note that due to the surface being relatively hydrophilic, we could still get some steric repulsion at higher temperatures. Therefore, no aggregation was observed at higher temperatures. We could also note that the stability of the dispersions was more pronounced at higher temperatures as a result of electrostatic repulsive interactions as compared to low temperatures where particles were sterically stabilized. The lower stability of particles at low temperatures were attributed to the effect of physically adsorbed or dissolved chains increasing the risk of aggregation. These chains were then detached from the (hydrophilic) surface (if present) as temperature increased, leading to an increased particle stability. Besides, the stronger hydrophobic interactions between chains at high temperatures were counteracted by strong electrostatic repulsive interactions which resulted in an increased stability. This prevented particles from displaying any thermoresponsive aggregation. Even though the particles were not thermoresponsive, the results of these experiments were still insightful, underlying the fact that the particle surfaces need to be hydrophobic in order to undergo temperature dependent aggregation. We, therefore, did not perform more measurements on thermoresponsive properties using carboxylated PS particles. We note that at higher particle concentration or larger graft thickness, we could observe temperature-dependent aggregation. We also note that the pH varied from 5 to 6 upon pegylation. The zeta potential of carboxyl particles at a fixed size, even though differing in the size of core and thickness, was considerably larger, at least 6-7 times those we found for the synthesized particles, in our published work. This resulted in the creation of a strong repulsive barrier at elevated temperatures, preventing particles from aggregation. We also performed DFT calculations on particles with conditions similar to what was established in our research paper, but under the assumption of non-adsorbing particle surface, at high temperatures. Implementing the code, we arrive at a PMF containing only repulsive barriers which agrees well with the experimental observations showing no sign of aggregation. The PMF is illustrated in figure 5.10. The reduced temperature, T*, was varied from 6 to 8 corresponding to 179.2 °C and 66.14 °C. Hence, we could reach an attractive minimum at extremely high temperatures, which could then induce hydrophobic interactions between chains resulting in particle aggregation. However, this would require an unrealistically high temperatures in experiments.

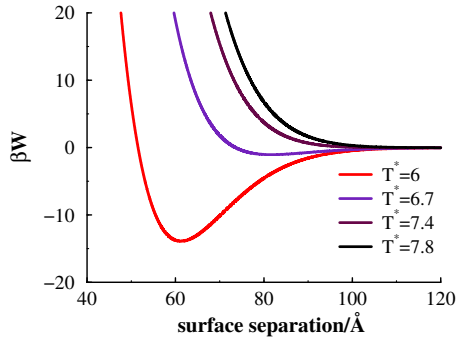

Figure 5.10: The simulation results of the potential of mean force at different T^*, the reduced temperature with 6 corresponding to 179 °C and 7.8 corresponding to 69 °C. Note: there is only grafted chains contributing the interactions. The double-layer repulsion was not included, but could be easily added.

5.6 Experimental study of carboxylated particles, depletion effect

The effect of depletion interactions on dispersions containing carboxylated particles has also been investigated. The aggregation behaviour and temperature-response were the focus of these analyses. Therefore, thermal analysis of samples were performed by heating the samples of particles dispersed in the aqueous solutions of dissolved PEG having MW of 100 kDa and imaging using a confocal microscope. Samples of particles with volume fraction of 0.06 and 0.1 were prepared followed by addition of PEG at concentration of 9 and 15 mg/ml. Samples were then kept at room temperature, and at 33 °C and 46 °C as well as 75 °C. The presence of PEG at sufficiently high amounts added, resulted in particle aggregation, due to depletion interactions. PEG is, at low temperatures, completely soluble in water, and do not adsorb to the rather hydrophilic carboxylated PS particle surfaces. The low concentrations of PEG chains in the interparticle region then generate attractive interactions, due to depletion forces. Further temperature raise resulted in even stronger particle association, to an extent that global phase separation occurred, leading to flocculation. The rate of sedimentation and phase separation was found to be dependent on temperature and concentration so that at 'small ranges', aggregation was a slow process whereas at large extremes, cluster formation was fast with particles rapidly growing in size, to form clusters which did eventually phase separate. In contrast to what we observed for the synthesized particles in our established work, we could not generate any redispersion or a non-monotonic temperature response, but rather a more pronounced aggregation upon temperature increase. We attribute this behaviour to the affinity of PEG toward the surface. The PS surface carried large amounts of surface charges, which was characterized by large values for the zeta-potential, generated from carboxylic acid grafts, creating a more

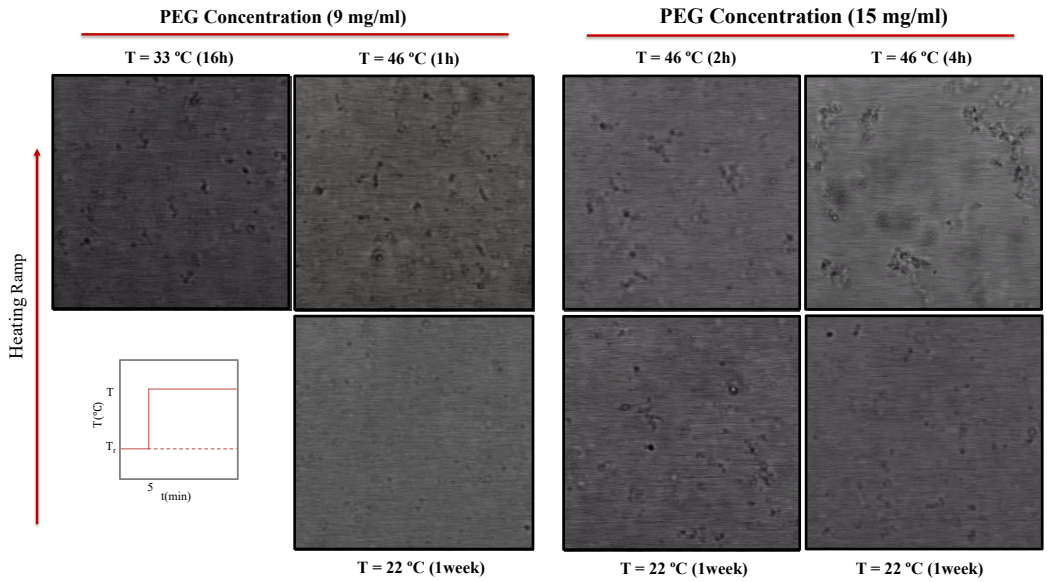

Figure 5.11: The thermal analysis of particles using confocal microscopy in the presence of added PEG at different concentrations. The thermal analysis is depicted using a heating ramp starting at T_r, the reference temperature to T, higher temperatures. The heating profile in dashed line shows that the particles are allowed to rest at T_r.

hydrophilic surface. Since the PS surface was hydrophilic and particles carried large number of surface charges, they therefore remained dispersed in the dispersions. In contrary to the synthesized PS grafted with PEG (in our published work), the surface of PS was here more hydrophilic, which resulted in desorption of PEG. The carboxylated ligands were also short for steric repulsion to have an impact, therefore particles were stabilized mainly due to the electrostatic repulsions which was counteracted by PEG-induced depletion interaction. The temperature raise resulted in PEG becoming increasingly hydrophobic. Hence the hydrophilic surface of PS was still not adsorbing the PEG, causing the depletion interactions to remain dominant, also at higher temperatures. This resulted in gradual aggregation. In contrast to what we observed for the synthesized particles (in our published work), the interactions were here dominated by attractive depletion forces, throughout the entire temperature range. This conclusion also finds support by a strong dependence on polymer concentration.

The polymer-mediated interactions were modelled using the same DFT we adopted in the research work, assuming that the surface is hydrophilic, i.e. hard but otherwise inert. This results in depletion interactions at all temperatures. The model could reasonably reproduce the results of experimental observations. The resulting PMF is illustrated in figure 5.12 showing only attractive interactions throughout the entire temperature range as dominated

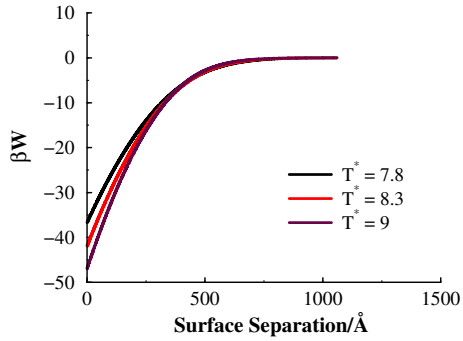

Figure 5.12: The simulation results of the potential of mean force at different T^*, the reduced temperature.

by depletion forces. The electrostatic repulsive forces could in principle also be added, using a PB-DFT for a better description of the model. However, as supported by the experimental results, we could note that the contribution of ES interactions to the particle aggregation were almost negligible.

5.7 Experimental study of CIPS in porous environments

Experimental investigation of CIPS in porous media is the subject of this section. Being a thermoresponsive polymer, PNIPAM is utilized for the experiments.[71] In our system, the capillaries are formed inside the tubular region inside densely packed silica rods. The pH-regulatory properties of silica allows us to adjust the hydrophobicity of surface, by using buffer solutions at different pH as the dispersing solvent.[72, 73] We study the effect of chain length, pH, and temperature on the interactions. We start by constructing the phase diagram of PNIPAM in a (bulk) buffer solution and continue to measure the effect from confined geometries on the phase diagram, where the silica rods are immersed in an aqueous solution containing polymers. We use magnetic resonance spectroscopy (NMR, in solid state) to measure the effect of capillary forces on phase transitions of PNIPAM, where changes in mobility of polymer chains at elevated temperatures due to the phase transitions cause a change in the chemical shifts. The decay of the intensity was considered as an indicator of a phase transition, with the inflection point of intensity against temperature being collected as the points on the cloud point curve. [74]

Solutions of PNIPAM with MW of 10 and 30 kDa at a varying concentration were prepared for the analyses. The NMR spectrum (peak intensity) for a bulk solution of PNIPAM at

temperatures below and above the cloud point is illustrated in figure 5.13. The intensity of the peak at 1.2 ppm, corresponding to the methyl group in the polymer backbone, varied as temperature increased. The intensity of the peaks were then monitored at each temperature by calculating the area under the peaks, plotted in figure 5.14. The reduced intensity was associated to a change in chain mobilities which occurred due to phase transition, decreasing to a point where broadening and further vanishing of peaks were indications of the presence of a concentrated phase. This was then referred to as a cloud point. The solutions in the presence of silica, i.e. capillaries, were analyzed in an analogous manner.

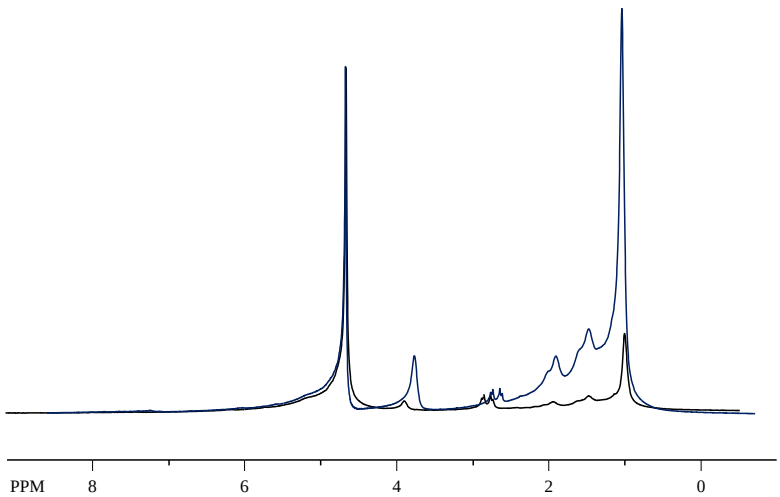

Figure 5.13: The NMR spectra of the bulk PNIPAM (10 kDa) solution in the absence of silica below and above the phase transition temperature.

The phase diagram was constructed by finding the transition points at various concentrations, where its minimum was referred to as the LCST of the polymer solution. The phase diagram of PNIPAM 10 kDa in buffer solutions are shown, together with the intensity graphs, in figure 5.14. The intensity graph of bulk samples indicates that the plateau region for concentrated samples is shifted upward, as compared to the dilute cases, indicating that while a majority of the molecules remain insoluble after the transition, a fraction of liquid-like molecules still remained dissolved, contributing to the values at the plateau region. We note that going from left to right on the phase diagram curve (U-shape), from dilute to concentrated region, the z-shape intensity curve turns to straight line, showing no transition for concentrated samples. This is in fact due to cohesion between chains and the entanglements present within the polymeric matrices. The transition temperature was reduced at the intermediate regimes, meaning that the transition occurred faster for these samples, which was due to the cooperative effects and hydrophobic interactions between polymer

chains. We could not detect significant changes to the phase transition of PNIPAM 30 kDa in the presence of silica. The main reason for this might be that the tubular region inside the hollow silica rods were too narrow to accomodate polymers. Furthermore, the data found for the transition in the presence of rods/short chains were not completely consistent (significant scatter), but we could find values below LCST for samples with high concentrations. The main parameters changing the results here were the spacing gap within rods, and the concentration of the solutions. This study aimed at a qualitative investigation of CIPS to see whether decrease in the value of LCST occurs within rods or not, hence it suffices here to state that we could collect points below the LCST, even though this effect may not be statistically significant. The decrease in the intensity was generally smaller in the samples containing rods. This might indicate that the mobility of chains in the dilute state is lower inside the capillaries that in the bulk, so that the decrease in the mobility associated with the phase transition is less pronounced. The schematic representation of system is illustrated in figure 5.15.

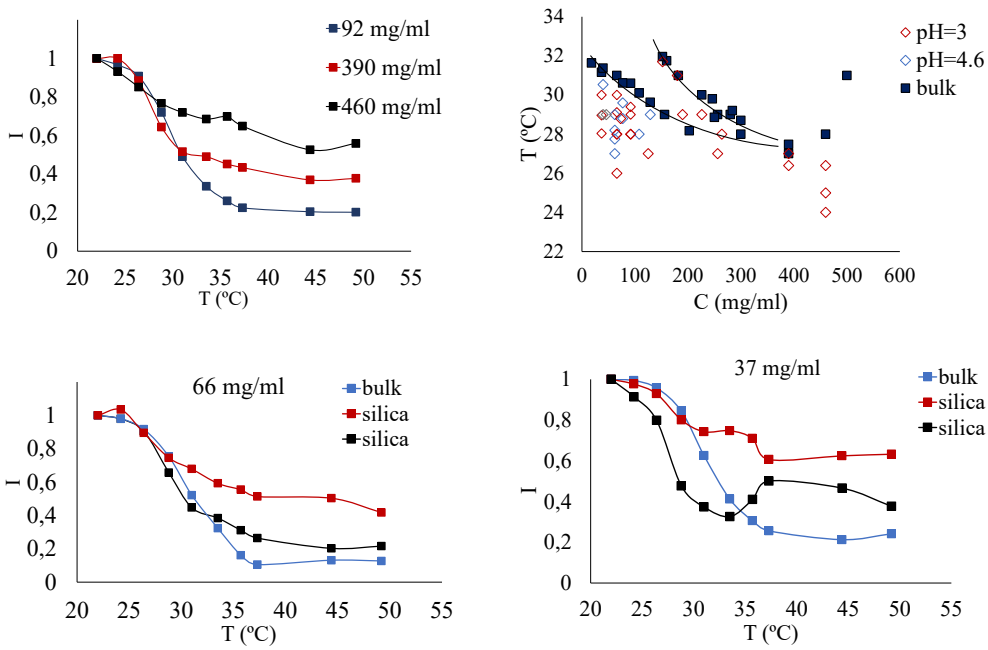

Figure 5.14: The phase diagram and the intensity graphs showing the phase transitions of PNIPAM (10 kDa). The values shown in the plots are the concentration of bulk samples.

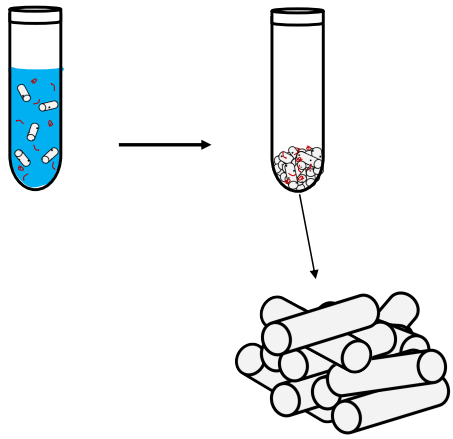

Figure 5.15: The schematic representation of the geometry created for CIPS study.

References

[1] M.M. Van Schooneveld, V.W.A. Villeneuve, Roel Dullens, Dirk Aarts, Mirjam Leunissen, and Willem Kegel. Structure, stability, and formation pathways of colloidal gels in systems with short-range attraction and long-range repulsion. *The journal of physical chemistry. B*, 113:4560–4, 05 2009.

[2] Elizabeth Elacqua, Xiaolong Zheng, Cicely Shillingford, Mingzhu Liu, and Marcus Weck. Molecular Recognition in the Colloidal World. *Accounts of Chemical Research*, 50(11):2756–2766, 2017.

[3] Francesco Sciortino, Stefano Mossa, Emanuela Zaccarelli, and Piero Tartaglia. Equilibrium cluster phases and low-density arrested disordered states: The role of short-range attraction and long-range repulsion. *Physical review letters*, 93:055701, 08 2004.

[4] Francesco Sciortino, Piero Tartaglia, and Emanuela Zaccarelli. One-dimensional cluster growth and branching gels in colloidal systems with short-range depletion attraction and screened electrostatic repulsion. *The journal of physical chemistry. B*, 109:21942–53, 12 2005.

[5] Lara Frenzel, Felix Lehmkühler, Michael Koof, Irina Lokteva, and Gerhard Grübel. The phase diagram of colloidal silica-pnipam core-shell nanogels. *Soft Matter*, 16(2):466—475, 11 2019.

[6] Jeanette Ulama, Malin Zackrisson Oskolkova, and Johan Bergenholtz. Monodisperse PEGylated spheres: An aqueous colloidal model system. *The Journal of Physical Chemistry Part B*, 118(9):2582–2588, 2014.

[7] Jeanette Ulama, Malin Zackrisson Oskolkova, and Johan Bergenholtz. Polymer-graft-mediated interactions between colloidal spheres. *Langmuir*, 32(12):2882–2890, 2016.

[8] Kaka Zhang, Ming Jiang, and Daoyong Chen. Self-assembly of particles - The regulatory role of particle flexibility, 2012.

[9] Jasper N Immink, J J Erik Maris, Jérôme J Crassous, Joakim Stenhammar, and Peter Schurtenberger. Reversible formation of thermoresponsive binary particle gels with tunable structural and mechanical properties. *ACS nano*, 13 3:3292–3300, 2019.

[10] Venkat Ganesan and Arthi Jayaraman. Theory and simulation studies of effective interactions, phase behavior and morphology in polymer nanocomposites, 11 2013.

[11] Pinar Akcora, Hongjun Liu, Sanat Kumar, Joseph Moll, Yu Li, Brian Benicewicz, Linda Schadler, Devrim Acehan, Athanassios Panagiotopoulos, Victor Pryamitsyn, Venkat Ganesan, J. Ilavsky, Pappanan Thiyagarajan, Ralph Colby, and J. Douglas. Anisotropic self-assembly of spherical polymer-grafted nanoparticles. *Nature materials*, 8:354–9, 05 2009.

[12] Anne-Caroline Genix and Julian Oberdisse. Nanoparticle self-assembly: From interactions in suspension to polymer nanocomposites. *Soft Matter*, 14, 06 2018.

[13] Siqi Liu, Erkan Senses, Yang Jiao, Suresh Narayanan, and Pinar Akcora. Structure and entanglement factors on dynamics of polymer-grafted nanoparticles. *ACS Macro Letters*, 5:569–573, 04 2016.

[14] Yang Jiao, Javier Parra, and Pinar Akcora. Effect of ionic groups on polymer-grafted magnetic nanoparticle assemblies. *Macromolecules*, 47(6):2030–2036, 2014.

[15] Yang Jiao and Pinar Akcora. Assembly of polymer-grafted magnetic nanoparticles in polymer melts. *Macromolecules*, 45(8):3463–3470, 2012.

[16] Understanding the role of grafted polystyrene chain conformation in assembly of magnetic nanoparticles. *Physical review*, 2014.

[17] Fuduo Ma, Xingfu Yang, and Ning Wu. Directed assembly of anisotropic particles under external fields. pages 131–165. 01 2018.

[18] Kouta Sugikawa, Tatsuya Kadota, Kotaro Matsuo, Kazuma Yasuhara, and Atsushi Ikeda. Growth of anisotropic gold nanoparticle assemblies via liposome fusion. *Materials*, 10:1317, 11 2017.

[19] Jurriaan Luiken and Peter Bolhuis. Anisotropic aggregation in a simple model of isotropically polymer-coated nanoparticles. *Physical review. E, Statistical, nonlinear, and soft matter physics*, 88:012303, 07 2013.

[20] Debapriya Banerjee, Beth A Lindquist, Ryan B. Jadrich, and Thomas M Truskett. Assembly of particle strings via isotropic potentials. *The Journal of chemical physics*, 150 12:124903, 2019.

[21] P Segrè, Vikram Prasad, Andrew Schofield, and D Weitz. Glasslike kinetic arrest at the colloidal-gelation transition. *Physical review letters*, 86:6042–5, 07 2001.

[22] Anna Stradner, Helen Sedgwick, Frédéric Cardinaux, Wilson C.K. Poon, Stefan U. Egelhaaf, and Peter Schurtenberger. Equilibrum cluster formation in concentrated protein solutions and colloids. *Nature*, 432:492–5, 12 2004.

[23] J. S. Shay, R. J. English, R. J. Spontak, C. M. Balik, and S. A. Khan. Dispersion polymerization of polystyrene latex stabilized with novel grafted poly(ethylene glycol) macromers in 1-propanol/water. *Macromolecules*, 33(18):6664–6671, 2000.

[24] Jennifer S. Shay, Srinivasa R. Raghavan, and Saad A. Khan. Thermoreversible gelation in aqueous dispersions of colloidal particles bearing grafted poly(ethylene oxide) chains. *Journal of Rheology*, 45(4):913–927, 2001.

[25] Dinesh Shenoy, Steven Little, Robert Langer, and Mansoor Amiji. Poly(ethylene oxide)-modified poly(??-amino ester) nanoparticles as a ph-sensitive system for tumor-targeted delivery of hydrophobic drugs. 1. in vitro evaluations. *Molecular pharmaceutics*, 2:357–66, 10 2005.

[26] Li Zhang, Eric Daniels, Victoria Dimonie, and Andrew Klein. Synthesis and characterization of pnipam/ps core/shell particles. *Journal of Applied Polymer Science*, 118:2502 – 2511, 12 2010.

[27] Malin Zackrisson, Anna Stradner, Peter Schurtenberger, and Johan Bergenholtz. Structure, dynamics, and rheology of concentrated dispersions of poly(ethylene glycol)-grafted colloids. *Phys. Rev. E*, 73:011408, Jan 2006.

[28] Matthew I. Gibson and Rachel K. O'Reilly. To aggregate, or not to aggregate? considerations in the design and application of polymeric thermally-responsive nanoparticles.

[29] F. Sciortino, P. Tartaglia, and E. Zaccarelli. One-dimensional cluster growth and branching gels in colloidal systems with short-range depletion attraction and screened electrostatic repulsion. *The Journal of Physical Chemistry B*, 109(46):21942–21953, 2005. PMID: 16853852.

[30] Andrew I. Campbell, Valerie J. Anderson, Jeroen S. van Duijneveldt, and Paul Bartlett. Dynamical arrest in attractive colloids: The effect of long-range repulsion. *Phys. Rev. Lett.*, 94:208301, May 2005.

[31] Matti M. van Schooneveld, Volkert W. A. de Villeneuve, Roel P. A Dullens, Dirk G. A. L. Aarts, Mirjam E. Leunissen, and Willem K. Kegel. Structure, stability, and formation pathways of colloidal gels in systems with short-range attraction and long-range repulsion. *The Journal of Physical Chemistry B*, 113(14):4560–4564, 2009.

[32] Gianpietro Malescio and Giuseppe Pellicane. Stripe phases from isotropic repulsive interactions. *Nature materials*, 2:97–100, 03 2003.

[33] Gunnar Karlström. A new model for upper and lower critical solution temperatures in poly(ethylene oxide) solutions. *The Journal of Physical Chemistry*, 89(23):4962–4964, 1985.

[34] Manuel Romero-Cano and Antonio Puertas. Phase behaviour of a model colloid–polymer mixture at low colloid concentration. *Soft Matter*, 4, 05 2008.

[35] Jan Forsman and Clifford E. Woodward. Surface forces at restricted equilibrium, in solutions containing finite or infinite semi-flexible polymers. *Macromol*, 40:8396, 2007.

[36] Fei Xie, Clifford E Woodward, and Jan Forsman. Non-monotonic temperature response of polymer mediated interactions. *Soft Matter*, 2015.

[37] Fei Xie, Clifford E. Woodward, and Jan Forsman. Theoretical Predictions of Temperature-Induced Gelation in Aqueous Dispersions Containing PEO-Grafted Particles. *Journal of Physical Chemistry B*, 120(16):3969–3977, 2016.

[38] Lang Feng, Bezia Laderman, Stefano Sacanna, and Paul Chaikin. Re-entrant solidification in polymer–colloid mixtures as a consequence of competing entropic and enthalpic attractions. *Nat Mater*, 14(1):61, 2015.

[39] Dafne Musino. *Impact of surface modification on the structure and dynamics of silica-polymer nanocomposites*. Theses, Université Montpellier, November 2017.

[40] Miguel Gisbert-Garzarán, Miguel Manzano, and María Vallet-Regí. ph-responsive mesoporous silica and carbon nanoparticles for drug delivery. *Bioengineering*, 4:3, 01 2017.

[41] Mykyta Onizhuk, Anton Panteleimonov, Yu Kholin, and Vladimir Ivanov. Dissociation constants of silanol groups of silic acids: Quantum chemical estimations. *Journal of Structural Chemistry*, 59:261–271, 03 2018.

[42] Sanna Björkegren, Lars Nordstierna, Anders Törncrona, and Anders Palmqvist. Hydrophilic and hydrophobic modifications of colloidal silica particles for pickering emulsions. *Journal of Colloid and Interface Science*, 487:250–257, 2017.

[43] Martin Olsson, Per Linse, and Lennart Piculell. Influence of added particles on the phase behavior of polymer solutions. analysis by mean-field lattice theory. *Langmuir*, 21(23):10862–10870, 2005.

[44] Jeong-Gil Choi, D. D. Do, and H. D. Do. Surface diffusion of adsorbed molecules in porous media: monolayer, multilayer, and capillary condensation regimes. *Industrial & Engineering Chemistry Research*, 40(19):4005–4031, 2001.

[45] Baoxing Xu, Yu Qiao, Taehyo Park, Moonho Tak, Qulan Zhou, and Xi Chen. A conceptual thermal actuation system driven by interface tension of nanofluids. *Energy Environ. Sci.*, 4:3632–3639, 08 2011.

[46] Håkan Wennerström, Krister Thuresson, Per Linse, and Eric Freyssingeas. Long range attractive surface forces due to capillary-induced polymer incompatibility. *Langmuir*, 14:5664, 1998.

[47] Martin L. Olsson, P. Linse, and Lennart Piculell. Capillary-induced phase separation in binary and quasi-binary polymer solutions. a mean-field lattice study. *Langmuir*, 20:1611–1619, 2004.

[48] Martin Olsson, Fredrik Joabsson, and Lennart Piculell. Particle-induced phase separation in quasi-binary polymer solutions. *Langmuir*, 20(5):1605–1610, 2004.

[49] Sara Haddadi, Clifford E. Woodward, and Jan Forsman. Confinement-induced fluid-fluid phase transitions in simple fluid mixtures, under bulk supra-critical conditions. *Fluid Phase Equilibria*, 540, 2021.

[50] Fei Xie, Clifford E. Woodward, and Jan Forsman. Fluid−fluid transitions at bulk supercritical conditions. *Langmuir*, 29(8):2659–2666, 2013.

[51] Xin Min, Minghao Fang, Zhaohui Huang, Yan'gai Liu, Yaoting Huang, Ruilong Wen, Tingting Qian, and Xiaowen Wu. Enhanced thermal properties of novel shape-stabilized peg composite phase change materials with radial mesoporous silica sphere for thermal energy storage. *Scientific Reports*, 5, 2015.

[52] Waseem Aftab, Xinyu Huang, Wenhao Wu, Zibin Liang, Asif Mahmood, and Ruqiang Zou. Nanoconfined phase change materials for thermal energy applications. *Energy Environ. Sci.*, 11:1392–1424, 2018.

[53] Monika Schönhoff, Anders Larsson, Petra B. Welzel, and Dirk Kuckling. Thermoreversible polymers adsorbed to colloidal silica: a 1h nmr and dsc study of the phase transition in confined geometry. *The Journal of Physical Chemistry B*, 106(32):7800–7808, 2002.

[54] Illia Dobryden, Maria Cortes Ruiz, Xuwei Zhang, Andra Dėdinaitė, D. C. Florian Wieland, Françoise M. Winnik, and Per M. Claesson. Thermoresponsive pentablock copolymer on silica: Temperature effects on adsorption, surface forces, and friction. *Langmuir*, 35(3):653–661, 2019.

[55] T.L. Hill. *Statistical Mechanics*, pages 190, Eqn 30.20. Addison-Wesley, Reading, Mass., 1960.

[56] Sture Nordholm, Jan Forsman, Clifford Woodward, Ben Freasier, and Zareen Abbas. *Generalized van der Waals Theory of Molecular Fluids in Bulk and at Surfaces*. Elsevier, United States, September 2018.

[57] Wilson C. K. Poon, Angus D. Pirie, and Peter N. Pusey. Gelation in colloid–polymer mixtures. *Faraday Discuss.*, 101:65–76, 1995.

[58] Gregor Trefalt and Michal Borkovec. Overview of DLVO Theory. *Laboratory of Colloid and Surface Chemistry, University of Geneva*, 2014.

[59] Jacob N. Israelachvili. *Intermolecular and Surface Forces, 2nd Ed.* Academic Press, London, 1991.

[60] Kitty van Gruijthuijsen, Chantal Rufier, Ty Phou, Marc Obiols-Rabasa, and Anna Stradner. Light and neutron scattering study of peg-oleate and its use in emulsion polymerization. *Langmuir*, 28(28):10381–10388, 2012.

[61] Kitty van Gruijthuijsen, Marc Obiols-Rabasa, Marco Heinen, Gerhard Nägele, and Anna Stradner. Sterically stabilized colloids with tunable repulsions. *Langmuir*, 29(36):11199–11207, 2013.

[62] F. A. Evans and H. Wennerström. *The colloidal domain: where Physics, Chemistry, Biology and Technology meet*. VCH Publishers, New York, 1994.

[63] Clifford E." "Woodward. "density functional theory for inhomogeneous polymer solutions". *"J. Chem. Phys."*, "94":"3183", "1991".

[64] Daan Frenkel and Berend Smit. *Understanding Molecular Simulation: From Algorithms to Applications*. Academic Press, Inc., USA, 1st edition, 1996.

[65] Sara Haddadi, Hongduo Lu, Marcus Bäcklund, Clifford E. Woodward, and Jan Forsman. Polymer-like self-assembled structures from particles with isotropic interactions: Dependence upon the range of the attraction. *Langmuir*, 37:6052–6061, 2021.

[66] Tommy Garting and Anna Stradner. Synthesis and application of pegylated tracer particles for measuring protein solution viscosities using dynamic light scattering-based microrheology. *Colloids and Surfaces B: Biointerfaces*, 181:516–523, 2019.

[67] Sneha Kulkarni, Satishchandra Ogale, and Vijayamohanan Pillai. Tuning the hydrophobic properties of silica particles by surface silanization using mixed self-assembled monolayers. *Journal of colloid and interface science*, 318:372–9, 03 2008.

[68] J. Pawley. *Handbook of Biological Confocal Microscopy*. Springer US, 2013.

[69] R.F. Egerton. *Physical Principles of Electron Microscopy: An Introduction to TEM, SEM, and AEM*. Springer US, 2006.

[70] Bin Chen and J. Ilja Siepmann. Improving the efficiency of the aggregation-volume-bias monte carlo algorithm. *Journal of Physical Chemistry B*, 105(45):11275–11282, November 2001.

[71] Avraham Halperin, Martin Kröger, and Françoise M. Winnik. Poly(n-isopropylacrylamide) phase diagrams: Fifty years of research. *Angewandte Chemie International Edition*, 54(51):15342–15367, 2015.

[72] Miguel Gisbert-Garzarán, Miguel Manzano, and María Vallet-Regí. ph-responsive mesoporous silica and carbon nanoparticles for drug delivery. *Bioengineering*, 4:3, 01 2017.

[73] Roshan B. Vasani, Steven J. P. McInnes, Martin A. Cole, Abdul Mutalib Md Jani, Amanda V. Ellis, and Nicolas H. Voelcker. Stimulus-responsiveness and drug release from porous silicon films atrp-grafted with poly(n-isopropylacrylamide). *Langmuir*, 27(12):7843–7853, 2011.

[74] Monika Schönhoff, Anders Larsson, Petra B. Welzel, and Dirk Kuckling. Thermoreversible polymers adsorbed to colloidal silica: a 1h nmr and dsc study of the phase transition in confined geometry. *The Journal of Physical Chemistry B*, 106(32):7800–7808, 2002.

Scientific publications

Author contributions

Paper 1: Building polymer-like clusters from colloidal particles with isotropic interactions, in aqueous solution
I conducted all the experiments and wrote the first draft of this part of the manuscript. I also ran the initial parts of the simulations. I also participated in the analysis of the simulation results.

Paper 2: Polymer-Like Self-Assembled Structures from Particles with Isotropic Interactions: Dependence upon the Range of the Attraction
I ran simulations and performed structural analyses. I also participated in manuscript writing.

Paper 3: From Attraction to Repulsion to Attraction: Non-monotonic Temperature Dependence of Polymer-Mediated Interactions in Colloidal Dispersions
I conducted all the experiments and wrote the first draft of this part of the manuscript. I also ran calculations on systems of surfaces with grafted chains.

Paper 4: Confinement-induced fluid-fluid phase transitions in simple fluid mixtures, under bulk supra-critical conditions
I ran DFT calculations and produced the data for the plots in the paper. I also participated in the manuscript writing.

Printed by Media-Tryck, Lund 2021 NORDIC SWAN ECOLABEL 3041 0903

ISBN: 978-91-7422-893-9

Theoretical Chemistry
Department of Chemistry
Faculty of Science
Lund University